Manuscript Details

Manuscript number	DES_2018_2101
Title	Innovative desalination plant based on the use of renewable energy sources
Article type	Full Length Article

Abstract

The desalination of seawater is characterized by a wide use of fossil energy sources, with a considerable environmental impact. The technology presented in this paper has been named "Solar Desalination Geoassisted Continuous", an innovative system for salt and brackish water desalination, covered by an Italian patent, almost totally exploiting solar power and capable of producing distilled water with very low running costs compared to current technologies. The SDGC system effectively exploits film evaporation and is able to function only by integrating losses due to the non-ideality of the materials. Furthermore, it is built with elements that are commonly used in the building sector, which reduces construction costs. The results of the development have therefore led to a system that can be easily integrated in any context in which it is necessary to recover fresh water from a solution of salt or brackish water, for both potable uses and process uses.

Keywords	Desalination; Water; Renewable energy.
Corresponding Author	Guido Micheli
Corresponding Author's Institution	Politecnico di Milano
Order of Authors	Stefano Farné, Guido Micheli, Vito Lavanga, Manuele Giovanola
Suggested reviewers	Lilian Malaeb, Habib Ben Bacha, George Ayoub

Submission Files Included in this PDF

File Name [File Type]

2018 - DES - Desalination - Cover letter_2018_11_07.docx [Cover Letter]

2018 - DES - Desalination - Highlights_2018_11_07.docx [Highlights]

2018 - DES - Desalination - Main text_2018_11_07.docx [Manuscript File]

To view all the submission files, including those not included in the PDF, click on the manuscript title on your EVISE Homepage, then click 'Download zip file'.

Innovative desalination plant based on the use of renewable energy sources

Dear Editor(s),

Please accept this submission of a very detailed paper, of course longer than any usual submission: we really believe the content is rich and useful for the readers of your Journal.

Best regards,

The Authors

Abstract

The desalination of seawater is characterized by a wide use of fossil energy sources, with a considerable environmental impact. The technology presented in this paper has been named "Solar Desalination Geoassisted Continuous", an innovative system for salt and brackish water desalination, covered by an Italian patent, almost totally exploiting solar power and capable of producing distilled water with very low running costs compared to current technologies. The SDGC system effectively exploits film evaporation and is able to function only by integrating losses due to the non-ideality of the materials. Furthermore, it is built with elements that are commonly used in the building sector, which reduces construction costs. The results of the development have therefore led to a system that can be easily integrated in any context in which it is necessary to recover fresh water from a solution of salt or brackish water, for both potable uses and process uses.

Keywords: Desalination; Water; Renewable energy.

Biographical Notes:

Stefano Farné is a Contract Professor at Università di Pavia, Italy, where he holds the courses of Mechanical plants, Fluid machines and Logistics management in the degree courses of Industrial Engineering and of Industrial Automation Engineering. After the Master's degree in Industrial Technologies Engineering at Politecnico di Milano, he received his PhD at Politecnico di Torino. His main research fields and consultancy activities are Energy & Environment Management, Project Management, Quality & Logistics Management. He is a certified auditor for ISO 9001 and OHSAS 18001 management systems certification and a certified EGE (expert in energy management). He is the coordinator of the certification of the skills of the engineers of the Milan register and he is member of various commissions of the same professional association. He is Vice-President of the certification committee of IPMA Italy. He is the author of three books and of papers at national and international level.

Guido J.L. Micheli is an Assistant Professor of Industrial Plant Engineering at Politecnico di Milano, Italy, and he teaches in several international and domestic undergraduate, postgraduate, and Master courses. He holds a PhD with honours in Management, Economics and Industrial Engineering and an MSc in Mechanical Engineering. His main research fields and consultancy activities are Occupational Safety Management and Applied Ergonomics, Risk Assessment & Management, Supply Risk Management, Supply Chain Risk Management, and Green Industrial Management. He is the author of papers at national and international level on books, conference proceedings, and journals, including contributions in Safety Science, International Journal of Industrial Ergonomics, Applied Acoustics,

International Journal of Occupational Safety and Ergonomics, Risk Management, Management Decision, International Journal of Production Research, Production Planning & Control, Journal of Purchasing and Supply Management, and the International Journal of Physical Distribution and Logistics Management.

Lavanga Vito is graduated in Electrotechnics and in Nuclear Chemistry and has received a Degree in Mathematics; he has worked for 20 years in information systems, cognitive systems and neurosciences, collaborating with industrial and research groups (JRC, Sip / Telecom Italia, Eni / SNAM, RCS, Comit / Intesa); he has developed front and distance training platforms, innovations in digital and publishing (minidisk, spoken book, Payment / POS). He has elaborated and realized solutions for energy efficiency and sustainability, crowned by 10 patents granted on: biogas, algae, desalination, hydrogen extraction, capting electromagnetics radiative spectrum, light diffuser, fluid mixer, fluid separator, heating / cooling of large surfaces, redevelopment of thermal insulation absorber and thermal storage; based on its own patents and cooperating with third parties, he draws up sustainable projects dedicated to environmental and social sustainability, in "distributed and pervasive" assets dedicated to the energy autonomy and independence.

Manuele Giovanola received his Master Degree in Electrical Engineering from the Department Of Industrial and Computer Engineering of University of Pavia, Italy. Currently, he work in an Energy Service Company (Enertech Solution S.r.l.) located in Milan, Italy. In this company, he manages the electrical consulting sector and collaborates in the procurement sector, energy plant design and also in energy efficiency sector. He is a member of the Engineers Order of Milan, Italy, and he collaborates with Department of Industrial and Computer Engineering of University of Pavia.

Stefano Farné

Department of Industrial Engineering and Information Technology,

Università degli Studi di Pavia,

Via A. Ferrata, 5, 27100 Pavia – Italy

Email: stefano.farne@unipv.it

Guido J.L. Micheli*

Department of Management, Economics and Industrial Engineering,

Politecnico di Milano,

Piazza Leonardo da Vinci, 32, 20133 Milan – Italy

Email: guido.micheli@polimi.it

*Corresponding author

Vito Lavanga

Technical Direction of Energy Supply-Chain Plan Srl

Via Socrate 26, 20128 Milan - Italy

Email: areatecnica@escp.it

Manuele Giovanola

Technical Direction of Enertech Solution Srl

Via Giuseppina Lazzaroni 4, 20124 Milan - Italy

Email: manuele.giovanola01@ateneopv.it

Innovative desalination plant based on the use of renewable energy sources

Highlights

- ✓ A new technology is proposed, "Solar Desalination Geoassisted Continuous" (SDGC)
- ✓ SDGC uses renewable sources to produce almost all fresh water
- ✓ SDGC process recovers almost all latent heat, thanks to his patented thermal tunnel
- ✓ SDGC's operating costs account for half of a "traditional" technology operating costs
- ✓ SDGC's fresh water costs are about 45% less of MFS and more than 50% less than RO ones

Innovative desalination plant based on the use of renewable energy sources

Abstract

The desalination of seawater is characterized by a wide use of fossil energy sources, with a considerable environmental impact. The technology presented in this paper has been named "Solar Desalination Geoassisted Continuous", an innovative system for salt and brackish water desalination, covered by an Italian patent, almost totally exploiting solar power and capable of producing distilled water with very low running costs compared to current technologies. The SDGC system effectively exploits film evaporation and is able to function only by integrating losses due to the non-ideality of the materials. Furthermore, it is built with elements that are commonly used in the building sector, which reduces construction costs. The results of the development have therefore led to a system that can be easily integrated in any context in which it is necessary to recover fresh water from a solution of salt or brackish water, for both potable uses and process uses.

STATE OF THE ART

Desalination of sea water or brackish water is used in the production of drinking water, whose acceptable salinity limit is $500^{mg_{TDS}}/l$ (TDS: total dissolved solids), or in the production of demineralized water for industrial applications, such as the water used in steam boilers or power plants, where the level of salinity must be significantly lower, sometimes less than $10^{mg_{TDS}}/l$ (World Health Organization, 2017).

2.1 Characteristics of salt water

Sea water can be seen as a solution of fresh water and salts of various kinds, the quantity of which is not constant but is subject to variability depending on the location, the season and the surrounding anthropic activities. However, it can be stated that, on average, sea water has the following characteristics (Rognoni, 2010):
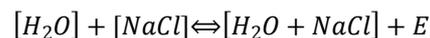- pH: $7.6 - 8.4$;
- Density at $20°C$: around $1025 \ kg/m^3$;
- Conductivity at $20°C$: $48,000 - 60,000 \ \mu S/cm$;
- Dissolved air: $20 - 28 \ ppm$;
- Salinity TDS: $34,000 - 45,000 \ ppm$.

Among the average parameters reported, the most important is certainly salinity, because it quantifies the total amount of dissolved salts. Based on this parameter, water is divided into four categories (Rognoni, 2010):
- Fresh water: $< 450 \ ppm$;
- Brackish water: $500 - 30,000 \ ppm$;
- Sea water: $30,000 - 50,000 \ ppm$;
- Brine: $> 50,000 \ ppm$.

2.2 References to the thermodynamics of desalination

The principle of sea water desalination is represented in the following chemical reaction: (Rognoni, 2010; Cipollina et al., 2009):

$$[H_2O] + [NaCl] \Leftrightarrow [H_2O + NaCl] + E$$

where E represents:
- dissolution heat: heat released during the melting of a salt in water;
- osmotic pressure: difference in pressure that is created when the osmotic membrane is placed between two solutions with different concentrations;
- ebullioscopic gradient: difference in evaporation temperature of a solution compared to pure solvent.

E therefore represents the minimum primary energy to be supplied so that transformation takes place and is independent of the process used, the value of which can be calculated by introducing a quantity of salt into a cubic meter of water sufficient to create a solution of water and salt equivalent to the marine one and measuring the increase in temperature due to the exothermic reaction. By performing this measurement, a temperature variation of about $0.64 \ °C$ is obtained, corresponding to $0.75 \ kWh/m^3$ (Rognoni, 2010; Cipollina et al., 2009).

To this value we must add the energy necessary to overcome the inefficiencies of technologies derived from the complex systems put in place to carry out the transformation.

2.3 Overview of the main existing technologies

This section will illustrate the main technologies adopted in common industrial practice, reporting some examples of plants in operation.

2.3.1 Evaporative plants

These are based on the evaporation of salt water and the subsequent condensation of humidified air using thermal or electric energy through conventional sources. In the more recent systems, however, a portion of the total energy is supplied by a solar energy system, thus constituting a hybrid system (Cipollina et al., 2009; Rognoni, 2010).

2.3.1.1 Multistage flash (MSF)

This is composed of a series of successive stages, each equipped with a heat exchanger and a condenser, maintained at decreasing pressure so that the temperature in each chamber is always kept above the boiling point (Figure 1).
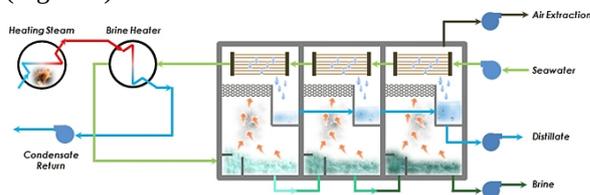

Figure 1. MSF plant layout (source: STX Heavy Industries)

The incoming water is pre-heated following the passage through the condensers present inside each stage at the expense of the thermal energy possessed by the steam inside the stage itself, which will be subject to a condensation process. Subsequently, the fluid is heated up to the saturation temperature after which it is sent to the first stage, where the temperature will be much higher than the internal pressure, causing a very rapid evaporation of a part of the salt water. The formed vapour will condense on the heat exchanger preheating the incoming water and the condensate produced will be conveyed to the outside. The remaining salt water will be at a lower temperature than the saturation temperature and will therefore be sent to the next stage, characterized by a higher degree of depression, repeating the process. (Cipollina et al., 2009).

The following is some data concerning existing plants in which significant use of solar energy has been used (Tzen, Zaragoza, & Alarcòn Padilla, 2012, p. 534):

- Lampedusa (Italy): powered by $408\ m^2$ of solar panels, produces $7.2 m^3/d$;
- San Luiz de la Paz (Mexico): powered by $194\ m^2$ of conventional solar panels and by $160\ m^2$ of concentrating solar panels, produces $10\ m^3/d$;
- El Paso (Texas): formed by the combination by $3355\ m^2$ of solar with a cogeneration plant. The plant produces electricity through a Rankine cycle and fresh water through a twelve-stage system. It produces $19\ m^3/d$ of fresh water.

2.3.1.2 Multiple effect distillation (MED or ME)

Taking advantage of the same principle adopted by the MSF technology, this uses a reactor instead of the vaporization chamber (Figure 2). The incoming water is preheated by the thermal energy contained in the steam
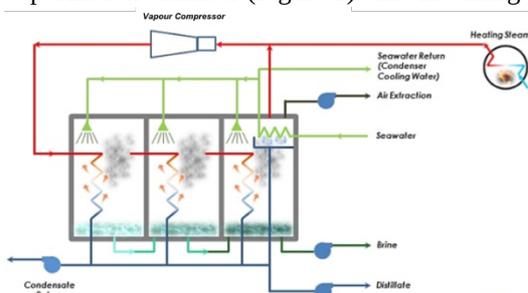

Figure 2. MED plant layout (source: STX Heavy Industries)

coming out of the last effect (or stage), after which it is sent simultaneously to the top of all the effects and diffused internally through suitable sprayers. Within each effect there is a heat exchanger that transfers thermal energy to the salt water but, of all the effects present in the system, only the first receives the energy directly from the heat generator; the other effects placed in the cascade receive energy through the steam formed in the previous effect, which transfers heat through the heat exchanger and condenses. Among all the effects present, therefore, the first will have the task of supplying the steam necessary for the whole process, while the task of producing the distillate will be entrusted to all the other subsequent effects (Cipollina et al., 2009).

There follows some data concerning existing plants (Tzen et al., 2012, p. 534):

- Abu Dhabi (EAU): powered by $1862\ m^2$ of solar panels, produces up to $120\ m^3/d$;
- Plataforma Solar de Almeria (Spain): powered by $500\ m^2$ of concentrating solar panels, produces $72\ m^3/d$.

2.3.2 Membrane processes

These create a separation between two fluids by applying a driving force to a selective barrier that is permeable only by some of the substances present in the fluid. The different types of processes are discriminated according to the source that produces the driving force: electrodialysis (exploits the action of an electric field), filtration (exploits a pressure gradient), osmosis (exploits the chemical potential), or dialysis (exploits the concentration gradient). Among these, the most commonly applied in the field of desalination is reverse osmosis; in the following we will also introduce the MD (membrane distillation) process, which is the most recent of all membrane processes.
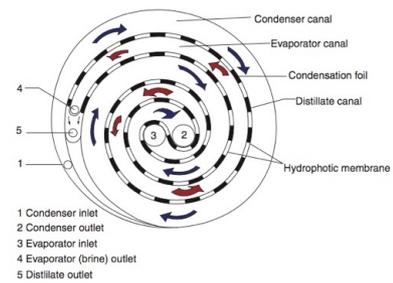

Figure 3. MD plant operating scheme (source: Tzen, Zaragoza, & Alarcòn Pasilla,

2.3.2.1 Reverse osmosis (RO)

The feed water is sent at high pressure to the high salinity compartment and flowed to the low salinity compartment of a semi-permeable membrane, reversing the osmosis process. The layout of the plant is relatively simple and consists of only a few elements (membranes, hydraulic pumps, pre-treatment systems and energy sources) but, nevertheless, this has become competitive only recently due to the cost of the membranes and maintenance. In fact, they are subject to fouling and incrustation caused by the precipitation of poorly soluble salts and this requires frequent maintenance. The efficiency of membrane removal varies according to the substances dissolved in the water, so a single stage is often not sufficient to give the finished product the necessary quality. The operating pressures are in the range of $50 - 80 \ bar$, beyond which it is possible to overcome the mechanical resistance of the membranes.

One of the most important plants is located at Lampedusa (Italy) (Tzen et al., 2012, p. 553): the system is able to provide $120 \ m^3/d$ of desalinated water through two RO units and the supply of electricity takes place via a $100 \ kW_p$ photovoltaic plant equipped with accumulation systems. The incoming water is pretreated, through filtration processes and through the introduction of chemical substances, to prevent fouling and corrosion phenomena and the salt content in the obtained water is lower than $500 \ ppm$, in compliance with the drinking water specifications established by the World Health Organization (Rognoni, 2010).

2.3.2.2 Membrane distillation (MD)

The incoming water is heated and evaporated, after which it comes into contact with a hydrophobic membrane that allows the passage of steam but not water. After passing through the membrane, the vapour comes into contact with a colder surface, where it condenses, producing fresh water that naturally flows towards the outlet of the system. The simplicity and the ability to operate with small differences in temperature make this a technology of considerable interest and, operating also at lower temperatures than the common distillation systems ($50 - 80 \ °C$), solar energy can be easily exploited (Figure 3).

Over time many pilot plants have been built and have given encouraging results. A $0.05 \ m^3/d$ desalination plant was built at New South Wales University in Australia; it exploits $3 \ m^2$ of solar panels. In the last ten years, several MD systems have been implemented within European projects (SODESA, MEMDIS and SMADES). The Fraunhofer Institut in Germany has developed compact solar MD modules that make it possible to achieve $10 - 30 \ l/h$ of distillate, working at $55 - 85 \ °C$ and providing $300 \ l/h$ of water in input. The system requires approximately $90 - 200 \ kWh/m^3$ of thermal energy and does not require inlet water pre-treatment systems (Tzen et al., 2012, p. 543).

Given the semi-experimental nature of this technology, the literature reports very wide energy consumption and fresh water costs ranges, between $1 - 9000 \ kWh/m^3$ and $0.28 - 123 \ €/m^3$ respectively (Reddy & Sharon, 2014, p. 1109).

2.3.3 Renewable sources processes

To date, around the world, to produce $1000 \ m^3/d$ of fresh water $10 \ kTOE/y$ are necessary, and that is why in recent years new systems powered by renewable sources have taken hold. The most commonly used sources in desalination are solar, wind and geothermal. Among these, the solar energy plays a particularly important role because it accounts for 57% of all production (Reddy & Sharon, 2014, p. 1081).

The systems shown below do not allow a particularly high production; however, they become competitive where there is a large availability of one of the renewable sources mentioned.

2.3.3.1 Solar chimney

This converts solar energy into kinetic energy of the air, which is in turn converted into electricity thanks to turboalternators. The system consists of a circular basin filled with salt water and covered with glass panels. The solar radiation that crosses the glazed surface develops within the phenomenon of the greenhouse effect. The heated air will therefore tend to go up the chimney, thus turning the wind blade installed transversely to the base of the chimney and connected to an electric generator (Figure 4).
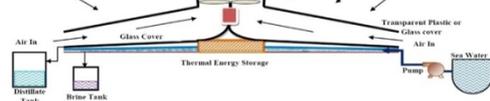
At the same time, the air that tends to rise along the chimney is in contact with the heated salt water present in the basin, which therefore tends to evaporate, increasing the internal humidity. The humidified air condenses in contact with a second glass plate characterized by a lower dew point temperature and the condensate is conveyed outside the plant. A variant of this system consists in removing the glass plate on which the steam condenses and replacing it with a high efficiency condenser placed on the top of the chimney, as shown in Figure 5.

Figure 5. Solar chimney plant layout (source: Reddy & Sharon, 2014)

Figure 4. Solar chimney variant plant layout (source: Reddy & Sharon, 2014)

Plants of this type have a production cost of about $2 \, €/m^3$ if they operate for $8 \, h/d$ (Reddy & Sharon, 2014, p. 1084).

2.3.3.2 Solar still

This plant is formed by a tank filled with salt water, closed on the top by a transparent glass plate, kept at a temperature below the dew point, that is able to allow the heating and the subsequent evaporation of the water present on the inside (Figure 6) as well as acting as a condenser for the system.
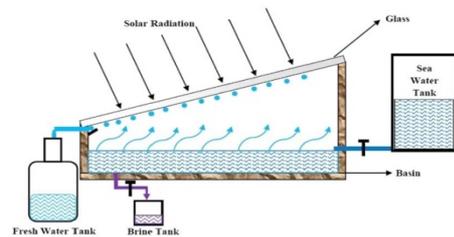
The main advantage of this system lies in its simple construction and the use of economically cheap materials; it also requires little maintenance. The simplicity, however, has some negative implications, represented by the low efficiency and low producibility. Although many studies are trying to improve their performance, most of these plants have an efficiency of around $30 – 45\%$, mainly due to the impossibility of recovering the latent heat of condensation, which is dissipated in the environment through the exchange plate; in addition, the production of fresh water is less than $5 \, l/m^2 d$. Studies on multiple effect systems have allowed a partial recovery of the latent heat, pushing the yield up to 57% and production up to $13 \, l/m^2 d$, obtained through the use of large mirrors to increase the incident solar radiation and the temperature inside the tank. However, this leads to greater plant complexity and higher costs.

Figure 6. Solar still plant layout (source: Reddy & Sharon, 2014)

A large solar still plant was installed in 1967 on the island of Patmos, Greece. The structure exploits a $8640 \, m^2$ basin and production is around $26 \, m^3/d$ (Tzen et al., 2012, p. 541; Reddy & Sharon, 2014, p. 1081).

2.3.3.3 Solar humidification–dehumidification (HDH or HD)

The humidity of an air flow is increased by circulating it through an evaporator in which heated salt water is sprayed. The humidified air is passed inside a condenser, from which the distillate is extracted (Figure 7). The system consists of a heater, a humidifier and a dehumidifier and the production potential depends essentially on the flow of air and the temperature of the feed water. Productivity can be increased through a cycle of water and air preheating and, to ensure maximum exploitation of the system, there is always an optimal relationship between the flow of air and the amount of water entering the humidifier, as a function of the water temperature entering the dehumidifier and that of the condenser. The most efficient configurations are represented by MEH, multi-effect
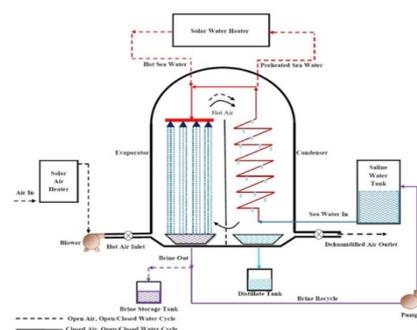

Figure 7. HDH plant layout (source: Reddy & Sharon, 2014)

systems in which the production cost of fresh water is around $3 - 7 \ €/m^3$ (Reddy & Sharon, 2014, p. 1083; Tzen et al., 2012, p. 544).

2.4 Literature review

Paragraph 2.3 presented the main technologies that are currently under the attention of researchers. From the analysis of the scientific literature on the subject, and filtering the results on the basis of technologies comparable to the SDGC system, it is clear how the topic is being treated in depth from the technological point of view, while it is lacking in studies that give an economic analysis to allow a better understanding of the situation. This is mainly due to the highly experimental nature of much of the research, which is too recent to be able to extend the analysis to the economic and technical feasibility.

The analysis shows that research on desalination systems, aimed at achieving production levels comparable with conventional technologies, finds fertile ground in HDH systems. Analysing the literature and comparing the various studies, it emerges that the common analysis data sees the main obstacle to the development of higher productivity in terms of distilled water. This aspect is dealt with in different ways: by improving the contact surface between the air and the water through the insertion of porous plastic elements to promote the humidification phase, as presented by (Chang, Zheng, Yang, Su, & Duan, 2014, p. 254), who were able to increase productivity to $63.6^{kg}/h$ with relatively contained specific costs of $4.4^{\$}/m^3$, or simply increasing the number of stages, as explored by (Hamed, Kabel, Omara, & Sharshir, 2014; Reddy & Sharon, 2014, p. 1081). In particular, the study on a double effect implant was developed by (Kang, Yang, Chang, Zheng, & Duan, 2014) in which, even through the reuse of condensation heat and the heat possessed in the brine, it is possible to reach a range of $72.6^{kg}/h$, at the expense of a considerable plant complexity compared to the solution proposed by (Chang et al., 2014, p. 254). A second solution is presented by (El-Agouz, Abd El-Aziz, & Awad, 2014, p. 278) and consists of a variation of the method by which the feed water is introduced into the system; by spraying it through a spray system instead of using a rain dispenser, the evaporation and condensation phase is encouraged, obtaining $9 \ l$ distilled flow rate per unit area of solar collectors installed at relatively low cost, in the order of $0.03^{\$}/l$. A third solution regarding the increase in the distilled product flow was analyzed by (Yildirim & Solmus, 2014, p. 570) and (Bacha, 2013), according to which it is possible to increase the performance of the system by increasing the flow of air entering the system up to a limit (optimal value) beyond which it is no longer possible to obtain benefits. The same study also denied the thesis of (Li, Yuan, Wang, Li, & Xu, 2014) according to which benefits could be obtained from preheating the incoming air for the purpose of increasing the relative humidity.

A second problem faced by the researchers mentioned concerns the uncertainty and the daily variability of productivity: the exclusive use of solar energy without accumulation systems to guarantee the needs (thermal and / or electric) causes a daily oscillation of the distillate flow rate, reducing its producibility. On the other hand, the integration of storage systems would increase total costs to the detriment of economic sustainability, but in the literature examined no comparative analyses were carried out to support this. The variability of the energy source is a problem that affects all renewable energy sources applied to any desalination technology; the study conducted by (Park, Schafer, & Richards, 2012, p. 867-874) specifically analyses the effect of power variability on a reverse osmosis desalination plant fed directly by a wind energy plant, showing how, in the absence of power supply, a passage of salt occurs through the membranes, reducing the quality of the product. From this we can understand how the continuity of the energy source is important not only for the quantity of daily product, but also for its quality.

At present, therefore, HDH systems are the ones most studied by researchers, who claim that systems of this type powered exclusively through renewable sources are applicable only on a small scale, due to the high investment cost, in relation to the production level reached.

In the literature there is also a limited contribution to the development of solar still systems: from the study carried out by (Manokar, Murugavel, & Esakkimuthu, 2014, p. 310) it emerges that the system is influenced by a number of variables that cannot be controlled by man, including the available solar radiation, humidity and environmental temperature, meteorological conditions, and wind speed, while the parameters on which we can act are plant orientation, roof inclination, construction materials and process temperatures. The studies also show that the main problem concerns the large surface necessary to ensure satisfactory producibility in passive systems which increases the total costs of planting. To compensate for the need for space reduction with the achievement of a satisfactory range, some solutions have been developed: the use of auxiliary systems to preheat the feed water and thus increase the production per unit area has been addressed by (Reddy & Sharon, 2014, p. 1081) through the use of solar collectors or with the aid of mirrors capable of increasing the incident radiation per unit area. The same study shows that the low performance of the plant is also due to the lack of recovery of latent condensation heat, which can only be used in multi-effect plants with significantly increased plant costs. A second study addressed by (Ayoub & Malaeb, 2014, p. 29) instead provides for increasing the evaporating surface by inserting a rotating cylinder into the system. The study argues that, according to the calculations

performed, with this system productivity can be improved by an order of $200 - 300\%$ compared to standard passive systems. This allows the reduction of the surface required for equal productivity; however, this solution is reflected in the specific production cost, which varies in the order of $6 - 30^{\$}/m^3$ and is higher than conventional passive systems due to the increased complexity of the system and therefore higher operating costs. Still in the field of technological solutions powered by renewable sources, (Reddy & Sharon, 2014, p. 1083) analyse the operation of solar chimneys, showing how, as a passive system, the operation cannot be prolonged efficiently beyond $8^{\,h}/d$, by virtue of the amount of useful solar radiation available. This is negatively reflected in the producibility and the specific production costs, evaluated by experimental plants as $2.23^{\$}/m^3$. The study also shows that the structure of these plants is large and very complex, which therefore implies high implantation and operating costs (not reported in the literature). To compensate for these costs, the system can be integrated with a series of wind turbines for the production of electricity.

Even traditional technologies, specifically the MSF plants, are being studied. These plants, typically adopted for high production, are generally fed from fossil sources. The aim of these studies is to replace conventional sources with economically sustainable technologies in the long run. The study conducted by (Reddy & Sharon, 2014, p. 1085) states that the use of MSF plants powered by solar energy can reach production orders up to 30 times higher than that achieved with solar still systems and with lower costs. Often, however, the energy produced by solar plants is not sufficient to cover the needs (given the randomness of the source itself) and they are therefore often coupled to power plants, in order to use the waste heat. An interesting study conducted by (Salata & Coppi, 2014, p. 614) plans to use solar ponds together with an absorption heat pump to preheat sea water to a temperature around $100\,°C$. According to the study, in fact, thanks to the high concentration gradients of the salts between the surface and the bottom of the solar ponds, there is a temperature inversion effect that brings the lowest layer of water to a higher temperature than that on the more superficial surface. Under the right conditions, solar ponds with depths of over one meter have a temperature difference of $50 - 60\,°C$, which maintains average values throughout the year (Ramadan, El-Sebali, Aboul-Enein, & Khallaf, 2004, p. 64), making it usable as a seasonal solar thermal energy collector. However, the study shows that, given the high surface area required for solar ponds, the system is only suitable for small-scale installations.

Another solution presented by (Kabeel & El-Said, 2013, p. 12) introduces a change to the MSF solar-powered system. By exploiting flash evaporation like traditional systems, it uses a heat carrier fluid enriched with nano-particles that favours the performance of the plant in terms of productivity. This makes the MSF system practicable on a small scale and it can reach specific levels up to $7.7^{\,l}/d$ per unit area of solar collectors. To date, estimated production costs are quite high, in the order of $11.7^{\$}/m^3$, and the installation costs (not shown) are mainly due to the cost of the collectors and of the water heating system. It is expected that increasing the performance of this portion of the system will reduce the specific cost by 63%.

The literature also reports some experimental plants built with the aim of obtaining an autonomous system that can be used to purify water in areas without adequate infrastructure for water supply. The study conducted by (Schafer, Remy, & Richards, 2004, p. 233-243) analyses the functioning of a desalination plant that combines solar technology with a membrane system, fed by waters with different chemical composition. The results show how, while using a simple and inexpensive system, the plant is able to produce drinking water with specific consumption varying between $5.5^{kWh}/m^3$ and $26^{kWh}/m^3$ according to the degree of salinity of the incoming water. The use of membranes, however, raises a series of problems due to the phenomenon of fouling that characterizes this technology and which increase the maintenance costs of the plant. Since the membrane technology is widely adopted, there are several studies that analyse this complication with the aim of limiting its effects: the analysis conducted by (Nam, Seockheon, Dooil, Seungkwan, & Ji, 2011, p. 1573-1579) studies the influence that the different materials constituting the membranes have on the phenomenon of dirtying them, while (Cervinia, Masaki, Tetsuji, Satoshi, & Wataru, 2016, p. 308-318) studies the effect of biofilm formation on the inorganic suspended solids accumulated inside the membranes, highlighting how a very thorough pre-treatment of the feed water is fundamental in membrane systems, to avoid further aggravating the membrane fouling.

The literature review presented in this section shows how the research on evaporative desalination systems powered by solar energy is full of potentially valid solutions, but that these still have some limits that have not been completely overcome. As can be deduced from the previous lines, researchers are grappling with the need to obtain satisfactory production levels while keeping the complexity of the system, and therefore the related costs, at economically sustainable levels.

From the solutions presented, we note how the superficial encumbrance of the systems is a limiting factor for the applicability of some large-scale systems, both for technical issues related to the possibility of realization, and for economic issues related to installation costs in relation to the production level obtainable.

Another critical issue concerns the operation of the plants: the exclusive exploitation of solar energy, without the addition of energy storage systems, makes the production of fresh water erratic and subject to weather conditions.

The randomness of solar energy, characteristic of all renewable sources, limits the operation of the plant to only daylight hours, thus increasing the cost per unit of production and compromising the quality.

The analysis of the state of the art therefore shows that the new systems fed through the exclusive exploitation of solar energy cannot yet be used for the desalination of large quantities of water. On the contrary, the integration of solar energy systems with traditional plants is the most satisfactory solution: as presented in paragraph 2.3.1, even if they do not reach the production levels of the technologies powered by conventional sources, they can produce up to a hundred daily cubic meters at a cost that would allow them to be used.

SDGC plant

The SDGC process (Solar Desalination Geoassisted Continuous) is an innovative thermal distillation process that is essentially based on a first humidification phase and a second phase of air dehumidification, exploiting, at steady state, only solar thermal energy.

As explained below, the development of this process is based on achieving a condition of equilibrium in which the only energy necessary for the system is provided to compensate for the inevitable inefficiencies, thus allowing the process of self-maintenance for a sufficiently long time to justify its industrial use.

3.1 Description

3.1.1 Plant structure

The system is made up of a reinforced concrete tank in the shape of a parallelepiped, thermally insulated by polyurethane foam panels to give it adiabatic characteristics, the inside of which is filled to about two thirds of the volume with the salt water to be treated.

In correspondence with the free surface of the plant, the tank is crossed by a series of corrugated pipes, made of materials characterized by a high thermal conductivity and connected to the system that will provide the main thermal energy and maintenance energy that will heat the salt water and maintain it at the established regimes.

Other corrugated pipes of the same material run through the tank at the top, bottom and side of the system; as will be explained below, these take on the function of reserve heat exchangers, able to intervene if a thermal equilibrium condition is reached in the system which, as will be explained in the following sections, represents a critical feature of the plant operation.

The whole tank is longitudinally crossed by a set of pressed sheets made of a material which is very thermally conductive and has an appropriate size and a predetermined percentage of vacuum / solid, such as to optimize the need for a sufficiently extended heat exchange surface while not hindering the movement of air. These plates are installed vertically in the central part of the tank, while they open to an accordion-like structure in the upper and lower part (Figure 8).

Near the free surface and up to a certain depth in the salt water, defined according to the temperature gradient between the free surface and the bottom of the tank so that the lower part is in contact with the coldest salt water, these sheets are compacted and thermally insulated with respect to the portion of water heated by the main heat exchanger, and the interstices formed by the reciprocal tiling are filled with liquid aluminum. This structure, called the thermal tunnel (Figure 8), represents a channel of communication between the two parts of the plant bordering a common area heated to a different temperature and, as explained in the following paragraphs, represents also the fulcrum of the whole system (Lavanga & Farné, Sistema di dissalatore geoassistito continuo, 2016).

In order to allow the process to develop with sufficient industrial speed, the whole tank is kept depressurised at predetermined levels and a suitable stirring system allows air to be supplied at the required speed in the portion of the tank not filled with salt water.

Figure 8. SDGC plant layoutFigure 8. SDGC plant structure

3.1.2 Working at full capacity

The operating principle is based on the heating of the salt water next to the free surface, while the water at the bottom remains at a lower temperature. During steady state operation, the free surface of the salt water is maintained at an average temperature of approximately $55 - 60\,°C$ by the solar thermal system, while the
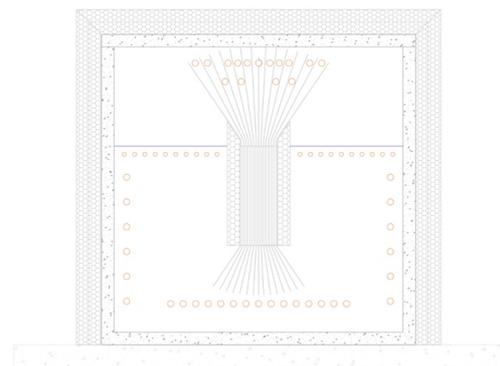
temperature at the bottom remains at around $15 - 25 \, °C$ (the temperature of the water entering the tank). This transversal temperature gradient recalls the operating principle of stratified accumulation systems used in plumbing and heating systems and is of fundamental importance for the functioning of our system, because it represents the real "engine" of the system. The point of entry of thermal energy is not random; in fact, the heating system delivery is located in the central part of the system, while the return is positioned near the walls of the tank. All this makes it possible to obtain a non-homogeneous temperature distribution at the free surface and this promotes the priming and maintenance of the rotary convective motions.
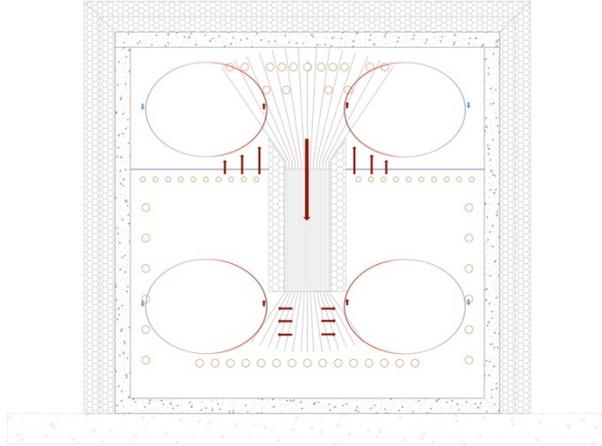

Figure 9. Convective motions and energy flows in the SDGC system

On the free surface of the tank, an evaporation process begins which, unlike boiling, has a lower speed and affects only the free surface of a fluid mass, as well as being visible at any temperature. Together with evaporation, on the free surface there is also a transfer of heat from the water to the air that allows the triggering of convective motions, promoted by the agitation system inside the tank. The greatest evaporation occurs near the central part of the system, due to the higher delivery temperature and, thanks to this, the air is charged with humidity. Furthermore, the vacuum setting of the tank further increases the evaporated flow rate.

The heated and humidified air, pushed upwards by convective motions and by the stirring system, comes into contact with the pressed metal sheets of the accordion structure. The latter, being in direct contact with the colder water at the bottom of the tank, are characterized by a lower temperature than the humidity of the humid air, so that in this phase the dehumidification process takes place by condensation of the steam in contact with the metal sheets. The condensate percolates on the pressed metal sheets up to a collection channel, to then be sent outside the plant.

In this phase the humid air gives heat to the sheets, which also includes the latent heat of condensation. Thanks to the thermal gradient between the upper part of the sheets, which is warmer due to dehumidification, and the lower part immersed in cold salty water, the absorbed heat is conveyed towards the lower part of the system through the thermal tunnel, where it is transmitted to the salt water and then completely recovered. Figure 9 shows the convective motions and the energy flows involved in the system.

As for the humidified air, as this gives up heat during the condensation phase, and its temperature continues to decrease to the point where it has reached a condition that causes it to move downwards.

Considering the submerged portion of the system, also in this area convective motions are formed. The heat given off by the sheets, in fact, heats the water at the bottom of the tank, which, thanks to the different density, rises back to the free surface, producing convective motions.

From this, the efficiency of the system is evident; in fact, unlike conventional systems, thanks to the maintenance of temperature gradients and the vacuum at the preset values, by supplying the initial thermal energy at the start of the process, the plant is able to sustain itself autonomously through the total recovery of latent condensation heat, integrating only the energy necessary to compensate for losses through the enclosure (Lavanga & Farné, Sistema di dissalatore geoassistito continuo, 2016).

3.1.3 Mathematical model of the process

The mathematical model that allows the analysis of the process and its design is presented below. The analysis was performed by decomposing the system and modelling the individual processes that occur during normal operation.

3.1.3.1 Evaporated flow rate

The evaporated flow rate from the free surface of the tank can be modelled through the convective diffusion equations. By definition, in the contact zone between a liquid and its own vapour, the saturation pressure applies, so the hygrometric degree (or relative humidity if expressed as a percentage, indicated below with the symbol "ϕ") expressed as the ratio between the partial pressure of water vapour p_{vap} and the saturation pressure of water at a given temperature p_v, is 1. This value will be constant throughout the system, since for operation it is not necessary to change the percentage of relative humidity in the air, but only the amount of water present. We call:

- p_{vap0}: partial pressure of water vapour on the free surface;
- p_{vapL}: partial pressure of the water vapour at such a distance as not to be disturbed by the effects that occur on the free surface (in the system, this is the top of the tank);

- $p_v(T)$: saturation pressure at temperature T (expressed in $°C$ or K, according to the calculation system or the table used to derive it).

As stated above, we can reasonably assume that the vapour pressure on the free surface is equal to the saturation pressure measured at the water temperature on the free surface, while the vapour pressure near the top of the tank will be equal to the saturation pressure evaluated at the dehumidified air temperature, since the hygrometric degree is everywhere unitary:

$$p_{vap0} = p_v(T_0)$$
$$p_{vapL} = p_v(T_L)$$

The water vapour spreads upwards with a partial pressure that decreases as the distance from the free surface increases. Diffusion is a phenomenon that manifests itself in space; however, we neglect the diffusion of water vapour downwards (when blocked by the presence of water) and towards the side walls (the vapour permeability of the walls is assumed to be negligible), to consider the one-dimensional vapour flow upwards (i.e. from the free surface of the tank towards the roof). On this premise, we can take advantage of the generalized Fick's Law (Farina, Santi & Lavacchielli, 2014, chapter 3, p. 4), with which one can express the molar flow of vapour per unit of surface that spreads in air:

$$\vec{N}_A = -CD_{AB} \cdot grad(x_A) + x_A\vec{N}_A \qquad \left[\frac{kmol}{m^2 s}\right] \qquad (1)$$

in which the first of the two addenda quantifies the phenomenon of diffusion, while the second one is transport of the matter. For the hypothesis about the directionality of the flow, we can simplify the relation in the case of one-dimensional flow:

$$N_{A_z} = -CD_{AB}\frac{dx_A}{dz} + x_A N_{A_z} \qquad \left[\frac{kmol}{m^2 s}\right] \qquad (2)$$

where:
- $N_{A_z}[kmol/m^2 s]$: molar flow of water;
- $C[kmol/m^3]$: concentration of the chemical species;
- $D_{AB}[m^2/s]$: binary diffusivity of water in air, evaluated at the water temperature on the free surface;
- $x_A[adim]$: molar fraction of the chemical species A (water vapour).

Explicating, we get:

$$N_{A_z}dz = -CD_{AB}\frac{dx_A}{1-x_A} \qquad \left[\frac{kmol}{ms}\right] \qquad (3)$$

and integrating formula (2) along the whole length of interest z results in:

$$N_{A_z}\underset{a}{\int_0^L dz} = -CD_{AB}\int_{x_{A_0}}^{x_{A_L}}\frac{dx_A}{1-x_A} \qquad \underset{b}{N_{A_z}L = CD_{AB}\ln\left(\frac{1-x_{vapL}}{1-x_{vap0}}\right)} \qquad \left[\frac{kmol}{ms}\right] \qquad (4)$$

in which L indicates the distance between the free surface and the tank cover. Recalling that, from Dalton's partial pressures law (that is, that the total pressure exerted by an ideal mixture of ideal gases is equal to the sum of the partial pressures that would be exerted by the gases if they were present alone in an equal volume), we have that $x_{as} + x_{vap} = 1$, the formulation becomes:

$$N_{A_z}L = CD_{AB}\ln\left(\frac{x_{asL}}{x_{as0}}\right) \qquad \left[\frac{kmol}{ms}\right] \qquad (5)$$

Assuming that both aeriforms (water vapour and dry air) behave like perfect gases, the following relationships can be applied:

$$\underset{a}{x_A = \frac{p_A}{p_{tot}}} \qquad \underset{b}{x_{as} = \frac{p_{as}}{p_{tot}}} \qquad \underset{c}{C = \frac{p_{tot}}{RT}} \qquad (6)$$

Substituting in formula (5) and applying to our system, we obtain:

$$N_{A_z} = \frac{p_{tot}D_{AB}}{RTL}\ln\left(\frac{p_{tot} - \phi p_{sat}(T_L)}{p_{tot} - \phi p_{sat}(T_0)}\right) \qquad \left[\frac{kmol}{m^2 s}\right] \qquad (7)$$

As stated at the beginning of the paragraph regarding the psychrometric state of the moist air inside the tank, the relationship (7) becomes:

$$N_{A_z} = \frac{p_{tot} D_{AB}}{RTL} \ln\left(\frac{p_{tot} - p_{sat}(T_L)}{p_{tot} - p_{sat}(T_0)}\right) \qquad \left[\frac{kmol}{m^2 s}\right] \qquad (8)$$

in which R is the universal constant of the perfect gases, while T represents the average temperature between the one near the covering and the one at the free surface of the tank, corresponding to a medium concentration. As will be seen in the following, this approximation will be irrelevant in the calculations.

From formulas (7) and (8), it can be seen how, in the case of an environment in saturation conditions (relative humidity equal to 100% or unit hygrometric degree), the evaporation speed depends essentially on the total pressure and the process temperatures which, influencing the saturation conditions, are fundamental for the good functioning of the plant.

Expressing the result in terms of mass flow and not of molar flow, the evaporated mass flow per unit of surface is obtained (Farina et al., 2014, chapter 7, p. 4):

$$\dot{m}_{H_2O} = N_{A_z} \mu_{H_2O} \qquad \left[\frac{kg}{m^2 s}\right] \qquad (9)$$

in which $\mu_{H_2O} = 18 \, kg/kmol$ is the molar mass of water.

Analysing the problem from the engineering point of view, we realise that in this type of equation the speed of the air inside the tank is not considered, which is a fundamental element for increasing the potential of the system. Therefore, stopping at this level of analysis would lead to poor results, because it is implicitly affirming that the air above the tank is stopped.

To increase the level of detail, we rely on the relations of technical physics, and in particular the analogy that exists between the heat exchange by convection and the exchange of matter by diffusion. Comparing the equations that regulate these exchanges, in fact, it is possible to find a correspondence between the heat exchange by convection, expressed through Fourier's law (as in Moran, Shapiro, Munson, & DeWitt, 2011. P. 466) and the exchange of matter between chemical species, regulated by Fick's law (Farina et al., 2014, chapter 4).

At an engineering level, when equations and physical laws are elaborated, we often try to compact them according to the "single number" rule; in other words, we try to create a relationship between two quantities through a coefficient. In the case of heat exchange, to process the Fourier equation, the single number widely used is the convection coefficient h, from which Newton's law derives (Moran, Shapiro, Munson, DeWitt, 2011, p. 468):

$$P = \overline{h}(T_p - T_{inf}) \qquad \left[\frac{W}{m^2}\right] \qquad (10)$$

in which:
- $\overline{h}[W/m^2 K]$: average value of the convection coefficient on the surface;
- $P[W/m^2]$: intensity of the specific heat flow;
- $T_p[K]$: contact temperature with the wall;
- $T_{inf}[K]$: temperature at a distance such that the effects due to the presence of the wall are not felt.

In reality, the convective coefficient varies according to the temperature difference, so the link between the power and the temperature difference is not linear. However, for common engineering problems a convective coefficient can be considered as averaged over a characteristic length and considering their linear link without making significant errors (Moran et al., 2014, p. 562).

Taking advantage of the analogy, one can express the law of convective diffusion in a similar way:

$$n_A = \overline{h}_m(\rho_{A_p} - \rho_{A_{inf}}) \qquad \left[\frac{kg}{m^2 s}\right] \qquad (11)$$

in which:
- $n_A[kg/m^2 s]$: flux intensity of the chemical species A (water);
- $\rho_{A_p}[kg/m^3]$: density of species A on the wall;
- $\rho_{A_{inf}}[kg/m^3]$: density of species A at a distance such that the effects due to the presence of the wall are not felt;
- $\overline{h}_m[W/m^2 K]$: average transport coefficient of matter in the diffusive field.

Like the previous one, this too is not a linear relation since the material transport coefficient is not an absolute constant.

Applying the equation to the model and exploiting the relation (9) and the equation of perfect gases, we can obtain:

$$\dot{m}_{H_2O} = \frac{\overline{h}_m \mu_{H_2O}}{R}\left(\frac{p_{vap0}}{T_0} - \frac{p_{vapinf}}{T_{inf}}\right) \qquad \left[\frac{kg}{m^2 s}\right] \qquad (12)$$

In order to determine the flow rate of evaporated water per surface unit, the coefficient of exchange of matter in the diffusion field must be determined. The thermal-diffusive analogy allows the problem to be approached analogously to the heat exchange, so it is possible to determine it by using some dimensionless numbers.
The first non-dimensional number needed is the Reynolds number, expressed as (Farina et al., 2014, chapter 4, p. 10):

$$Re_{L_c} = \frac{v_{inf} L_c}{v(T_{inf})} \qquad [adim.] \qquad (13)$$

This expresses the relationship between the forces of inertia and the viscous forces, and its items are:
- $v_{inf}[m/s]$: fluid speed;
- $L_c[m]$: characteristic size;
- $v(T_{inf})[m^2/s]$: kinematic viscosity at the temperature of the undisturbed current.

The Reynolds number is necessary to establish whether the process of convective diffusion takes place in a laminar or turbulent regime. From the literature, limiting the analysis to our process (approximated in these terms as a flat plate lapped by a moving fluid), the critical Reynolds number for which the transition from laminar to turbulent flow is considered is equal to 500,000, which is much greater than the transition value for cases of fluid flowing inside a pipe.
The second dimensionless number necessary for the analysis is the Schmidt number, expressed as (Farina et al., 2014, chapter 4, p. 11):

$$Sc = \frac{v(T_{inf})}{D_{AB}} \qquad [adim.] \qquad (14)$$

This expresses the relationship between the kinematic diffusivity and the diffusivity of matter and, compared to the thermal-diffusive analogy, is the equivalent of the Prandtl number. These items have already been explained in the previous pages.
The last non-dimensional number needed for the calculation is the Sherwood number, expressed as (Farina et al., 2014, chapter 4, p. 11):

$$\overline{Sh}_{L_c} = \frac{\overline{h}_m L_c}{D_{AB}} \qquad [adim] \qquad (15)$$

This represents the relationship between the convective and diffusive mass transfer and is the analog of the Nusselt number in the diffusive field. Equivalently to this, it is possible to express the Sherwood number according to the Reynolds and Schmidt numbers raised to appropriate coefficients, through Colburn's reports (Farina et al., 2014, chapter 6, p. 11).
Leaving to the literature the treatment of these relationships, there are only two that are of practical interest for the system under examination, one related to the laminar regime, the other relative to the turbulent one; the use of one or the other equation depends on the value of the Reynolds number, as stated on the previous page:

Laminar   Turbulent

$$\overline{Sh}_{L_c} = 0.664 Re_{L_c}^{1/2} Sc^{1/3} \qquad\qquad \overline{Sh}_{L_c} = (0.037 Re_{L_c}^{4/5} - 871)Sc^{1/3} \qquad (16)$$

$$a \qquad\qquad\qquad\qquad\qquad b$$

By obtaining the average convection coefficient through the dimensionless numbers, it is possible to easily calculate the evaporated flow per unit of surface according to formula (12) and, subsequently, to obtain the flow evaporated from the entire free surface of the tank through formula (12) (Farina et al., 2014).

3.1.3.2 Required power

In steady-state operation, the salt water temperature inside the tank is already at the process value. Therefore, as explained in the previous pages, the only thermal power to be introduced is that needed to overcome the losses through the casing.
In this regard, it is necessary to proceed considering that there are two fluids that interact with the heat exchange through the insulated walls of the tank. The part of the tank submerged by salt water will, in fact, contribute to the losses in a different way from the portion in the air. Moreover, during the design, the installation position of

the tank (underground, basement or external) must be taken into account in relation to the different materials that will contribute or not to the losses.

The specifics of the calculations will be presented in the following sections, while the following is the commonly adopted formula that allows us to calculate the losses through a stratigraphy (Moran et al., 2011, p. 495):

$$P_{tot} = \sum_{i=1}^{n} P_i \qquad [W] \qquad (16)$$

where P_i indicates the i-loss contributions determined by the different conditions inside and outside the tank exposed above, calculated as:

$$P_i = U_i A_i \Delta T_i \qquad [W] \qquad (17)$$

where the items are:
- $\Delta T_i [K]$: difference between the internal and external temperature related to the loss surface considered;
- $A_i [m^2]$: loss surface considered;
- $U_i [W/m^2 K]$: thermal transmittance of the stratigraphy related to the loss surface considered, evaluated on the basis of the standards UNI EN ISO 6946:2008 (Components and building elements - Thermal resistance and thermal transmittance - Calculation method) and UNI EN ISO 13370:2008 (Thermal performance of buildings - Heat transfer through the ground - Calculation methods).

If the envelope of the system is properly thermally insulated, this contribution can be very small (Moran et al., 2011).

3.1.3.3 Distillate production

For the evaluation of the amount of distillate produced, it is necessary to consider that, when operating and in the best operating conditions, the maximum condensable quantity is strongly dependent on the quantity of evaporated water and in any case it cannot condense more than the system is managing to evaporate (otherwise it means that the plant is "creating" water, which is obviously absurd).

The water vapour contained in the humidified air starts to condense as soon as it finds a surface with a temperature equal to or lower than its dew temperature, and this complicates the analysis of the model. As a first approximation, it is assumed that steam starts to condense only once the thermal equilibrium between water and steam has been reached (this means at the limit of the stopping of the evaporative phase, as reported in formula (12)); this is a very strong approximation but, while still awaiting real measurements, allows us to obtain a good result.

Under this hypothesis, through the diagrams or psychrometric calculators, we obtain the thermo-hygrometric values related to the initial and final conditions of the condensation phase. The specific value of condensed water is obtained through the following formula (Moran et al., 2011, p. 321):

$$\dot{m}_{H_2O_u} = \omega_2 - \omega_1 \qquad \left[\frac{kg_v}{kg_{as}}\right] \qquad (18)$$

in which the items represent:
- $\omega_2 [kg_{vap}/kg_{as}]$: specific humidity of the humidified air;
- $\omega_1 [kg_{vap}/kg_{as}]$: specific humidity of dehumidified air.

This value is necessary to calculate the flow of dry air, which in turn is necessary to determine the power developed during condensation and to size the exchange surface.

Under the previous hypotheses, therefore, the flow of dry air is evaluated with the following formula (Moran et al., 2011, p. 320):

$$\dot{m}_{as} = \frac{\dot{m}_{H_2O}}{\dot{m}_{H_2O_u}} = \frac{\dot{m}_{H_2O}}{\omega_2 - \omega_1} \qquad \left[\frac{kg}{s}\right] \qquad (19)$$

Subscripts "1" and "2" indicate the conditions of the humid air and must not be misunderstood; even if it represents the final state of the dehumidification phase, it has been decided to indicate with subscript "1" the dehumidified air because it corresponds to the initial condition before the humidification.

From the flow of dry air, through the well-known formula deriving from technical physics (Moran et al., 2011, p 320), it is possible to obtain the mass flow of humid air to be moved with the stirring system:

$$\dot{m}_{au} = \frac{\dot{m}_{as} R_i T_{au}}{p_{as}} \qquad \left[\frac{kg}{s}\right] \qquad (20)$$

in which:
- $\dot{m}_{as}[kg/s]$: mass flow of dry air;
- $p_{as}[Pa]$: partial pressure of dry air;
- $R_i[J/kgK]$: specific constant of dry air, equal to 287 $[J/kgK]$;
- $T_{au}[K]$: temperature of the moist air mixture.

Formulas are taken from (Moran et al., 2011).

3.1.3.4 Thermal tunnel

The model for calculating the thermal tunnel consists in evaluating the number of pressed sheets necessary for the system to produce the maximum quantity of condensate, corresponding to the quantity of evaporating water under certain operating conditions.

The base of the thermal tunnel is an area characterized by a high thermal conductivity, due to the flanking of all the expanded metal sheets. Having this characteristic, if placed in contact with the colder area of the plant (the water at the bottom of the tank), it can reasonably be deduced that its temperature, during normal operation, will not be very different from that at the bottom of the tank and, above all, it will remain constant during operation.

From this, we can think of the base of the thermal tunnel as a surface that must absorb a large quantity of thermal energy and, from the technical physics rules (Moran et al., 2011, p. 511), the expanded metal sheets can be seen as a finned surface which must promote such absorption. Therefore, we use the analysis models of the finned surfaces to evaluate the number of fins necessary to allow heat exchange.

The expanded metal sheets are produced in sheets of standard dimensions and the geometrical characteristics of interest for the calculation are:
- Commercial dimensions of the sheet $[m]$ and its surface $[m^2]$;
- Percentage value of the void on full $[m]$: this represents the percentage of perforated surface compared to the metallic one and can vary widely. As will be seen in the following sections, it is of fundamental importance for the success of the design.

As the literature teaches, the fins are generally continuous surfaces of conductive material. Therefore, in order to bring us back to the model, it is necessary to obtain the equivalent metallic surface of the pressed sheets, since it will only be that which carries out the heat exchange. Taking advantage of the data available, this is obtained with the following formula:

$$S_{ls_{eq}} = S_{ls}\left(1 - \frac{\%VP}{1 - \%VP}\right) \qquad [m^2] \qquad (20)$$

in which:
- $S_{ls}[m^2]$: commercial surface of expanded metal;
- $\%VP[\%]$: percentage value of void on full.

Through the equivalent metal surface, the geometry of the sheet metal pre-stretching is obtained, with which the number of fins (pressed sheets) is calculated, so that the heat exchange takes place.

From the literature, we know that the analysis of the fins is regulated by the calculation of some coefficients that allow a simplification of the calculations.

As regards their theoretical treatment, refer to the bibliography (Moran et al., 2011; Magrini & Magnani, 2009).

The "M" coefficient of the fin (Magrini & Magnani, 2009, p. 255) is as follows:

$$m = \sqrt{\frac{2h}{\lambda s}} \qquad [m^{-1}] \qquad (21)$$

where:
- $h[W/m^2K]$: convective coefficient;
- $\lambda[W/mK]$: thermal conductivity of the material constituting the expanded metal sheets;
- $s[m]$: thickness of pressed sheets.

The coefficients "A" and "B" of the fin (Magrini & Magnani, 2009, p. 255) are:

$$A = \frac{t_p - t_{amb}}{1 + \frac{\lambda m - h}{\lambda m + h}e^{-2mH_{ls}}} \qquad\qquad B = \frac{t_p - t_{amb}}{1 + \frac{\lambda m + h}{\lambda m - h}e^{2mH_{ls}}} \qquad [K] \qquad (22)$$

$$a \qquad\qquad\qquad\qquad\qquad b$$

with H_{ls} the height of the expanded metal, expressed in meters.

Once the coefficients have been defined, the unit thermal flow is evaluated through the single stretched sheet (Magrini & Magnani, 2009, p. 255):

$$P_u = -\lambda s l_{eq}(B-A)m \qquad\qquad \left[\frac{W}{fin}\right] \qquad (23)$$

in which l_{eq} is the equivalent length of the expanded metal.

To estimate the number of sheets, it is necessary to calculate the total thermal power absorbed by the sheets stretched during the condensation, obtainable by means of an energy balance such as (Moran et al., 2011, p. 329):

$$P = \dot{m}_{as}\left((H_{au_d} - H_{au_u}) + (\omega_2 - \omega_1)H_{H_2O}\right) \qquad [kW] \qquad (24)$$

whose items not already explained in the previous paragraphs are:

- $H_{au_d}[kJ/kg]$: enthalpy of humid air, dehumidified;
- $H_{au_u}[kJ/kg]$: enthalpy of humid air, humidified;
- $H_{H_2O}[kJ/kg]$: enthalpy of the condensate, treated as saturated liquid.

All enthalpy values can be obtained from the tables showing the properties of the air.

Having calculated the total power required for condensation, we calculate the number of fins necessary for thermal exchange to take place:

$$n_{fins} = \frac{P}{P_u} \qquad\qquad [fins] \qquad (25)$$

The number of fins must be appropriately placed at the base of the thermal tunnel considering the total size of the metal sheet, not the equivalent one used for the calculation.

Case study and sizing

In this section we apply the analysis model developed in the previous pages, hypothesizing the operating conditions that will allow us to obtain a producibility in terms of condensate that can be compared with the technologies shown in section 2. Everything is done by orienting towards the design of a standard model that can be representative of a subsequent economic analysis, trying wherever possible to use standardized elements and materials commonly used in industry.

4.1 Materials used

The following paragraph shows an extract of the most important materials chosen for the analysis of the case study.

4.1.1 Control volume

The tank in which the system is to be built must be large enough to allow the use of a surface that will allow the evaporation of an adequate quantity of water without causing the system to operate under particularly severe operating conditions. Furthermore, it must be deep enough to ensure that the right temperature gradient is maintained. The material constituting the tank must be resistant to corrosion caused by salt water, be able to maintain the pre-set vacuum level inside, and be easy to install.

Prefabricated reinforced concrete tanks were chosen, as commonly used in water treatment plants. For the case study, the model C-15 of the company Gazebo S.p.A. was chosen, for which the data of interest are reported in Table 1 (Gazebo S.p.A., 2013):

Capacity	m^3	50
Width*	cm	250
Length*	cm	950
Height*	cm	250
*External dimensions		

Table 1. External dimensions of Gazebo C-15

The company in question provides customers with the .dwg format files with all the measurements of the tank. Table 2 shows the internal measurements:

Width	cm	230
Length	cm	930
Height	cm	230

Table 2. Internal dimensions of Gazebo C-15

Figure 10 shows an example of a multiple installation of the type of tank used.

Figure 10. Example of tank used

4.1.2 Thermal insulation

The tank must be thermally insulated in order to minimize dispersion to the external environment. To isolate it, it was decided to use polyurethane foam panels and the GT model of the company Stiferite S.r.l. (Figure 11) was chosen. The technical data are shown in Table 3 (Stiferite S.r.l., 2017):

Thickness	mm	100
Thermal transmittance	W/m²K	0.23
Operating range	°C	[-40–110]

Table 3. Stiferite GT100 technical data

The panel is built with the sandwich technique, consisting of an insulating component in polyiso foam, expanded without using CFC or HCFC, coated on both sides with a Duotwin® Green system.

We chose to install two superimposed panels of a total thickness of $200\ mm$; this decision was motivated by economic considerations; in fact, in common building practice, $100\ mm$ panels are used more and, therefore,

Figure 11. Foam panel (source: Stiferite S.r.l.)

their use on a large scale makes them economically cheaper than a single double-thickness panel, as the latter is less widely used.

4.1.3 Internal piping

Inside the tank there is a main exchanger, which is needed to heat up and maintain the salt water at the right temperature (contributing to the reintegration of the energy lost through the casing), and two safety exchangers, which are needed to restore the necessary thermal gradients that, as explained in section 3, are the cornerstone of the whole system.

For both uses, it was decided to use corrugated copper pipes, in order to guarantee an adequate degree of turbulence in the heat-carrying fluid and therefore promote heat exchange. These pipes are produced by the company Pantani Divisione Tubi S.r.l. (Figure 12) (Pantani Divisione Tubi S.r.l.), which specializes in the construction of corrugated and finned pipes for heat exchangers.

In addition to the above reasons, it is thought that due to the turbulence inside the corrugated piping micro-vibrations are created, which, when transmitted to the water promote its evaporation.

Figure 12. Corrugated pipes (source: Pantani Divisione Tubi S.r.l.)

4.1.4 Expanded sheets - Thermal tunnel

The material of which the thermal tunnel is made is of particular importance since it directly influences the plant's potential in terms of distillate production.

The expanded metal is produced by a simultaneous process of cutting and lengthening sheets or rolls of solid sheet. This process creates rhomboidal openings in the raw material that allow the passage of air, fluids and light. Stretched metal is chosen due to the fact that this product is commonly used in industry, so it costs less than other solutions that require tailor-made craftsmanship; moreover, it is a product that lends itself easily to the main mechanical processes such as bending, cutting, welding.

For the case study, a expanded metal with rhomboidal mesh was chosen, produced by the company Fratelli Mariani S.p.A. and having the characteristics shown in Table 4 (Figure 13) (Fratelli Mariani S.p.A.):

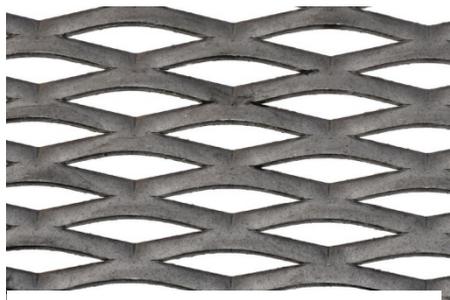| Material	//	Aluminum
Thickness	mm	2
Type of carving	//	Rhomboidal
Carving measures	mm	62 x 20
Empty on full	%	30%
Sheet measurements	mm	1000 x 2000

Table 4. Expanded metal technical data

Figure 13. Expanded metal (source: Fratelli Mariani S.p.A)

Near the free surface, the pressed sheet metal side by side must constitute a region with a high thermal conductivity that can dispose of the heat in an efficient way, so as to allow a sufficiently rapid condensation process. To guarantee this function, near the free surface the sheets will be separated from the salt water through polyurethane foam panels (coated with aluminum to protect against salt corrosion) forming a compact sheet packet.

The ideal condition of heat transmission could be pursued if, when passing through the thermal tunnel, the sheet is interrupted, to resume near the salt water on the bottom of the tank. However, in this first phase, as mentioned at the beginning of the section, we tried to obtain a satisfactory result using standardized materials, therefore, to fill the interstices that will inevitably be formed in the package of sheet metal side by side, we will inject liquid aluminum inside the structure.

4.1.5 Air stirring system

To achieve adequate process speeds, it is necessary that the convective motions developed inside the tank are characterized by a rather high speed, so as to push the evaporation and condensation phases to the maximum.
To obtain this result it is possible to use tangential stirring systems powered by electric motors. In the future it will be possible to evaluate the feasibility of using the patented MHML™ mixing system; it consists of the appropriate assembly of materials commonly used in industry, such as draining and circulating tubes. The advantage of this solution consists in the simplicity of installation and in the drastic reduction of the energy dispersions typical of vortical processes (Lavanga & Farnè, MHLM, 2017).

4.2 Sizing

The following section presents the result obtained following the application of the mathematical model analysed in section 3.
All design choices have been carefully evaluated with the aim of achieving a good compromise between performance and production and operating costs.

4.2.1 Operating conditions

After some preliminary calculations, we have seen how a good level of productivity was achieved through the implementation of the following measures:
- Work in vacuo;
- Artificial movement of indoor air;
- Adequate operating temperatures;
- Adequate evaporating surface: this condition is directly reflected in the size of the plant to be dedicated to the thermal tunnel;
- Transversal and longitudinal gradients: for optimal functioning, the distribution of salt water temperatures must be characterized by the formation of gradients between the free surface and the bottom of the tank (obtained through the stratification of the water) and between the center of this last and the side walls (obtained through the appropriate arrangement of the delivery and return of the system).

Table 5 shows the operating conditions taken into consideration for the application of the calculation model:

Total pressure inside the tank	Pa		30,000.00
Average salt water temperature in steady state (free surface)	°C		60.00
Humidified air temperature	°C		60.00
Dehumidified air temperature	°C		30.00
Total evaporating surface	m²		16.74
Humid air speed	m/s		9.00

Table 5. Operating conditions of the SDGC system

Salt water is heated only near the free surface and only to the extent that it guarantees evaporation without achieving thermal equilibrium, a condition whereby the system would stop. The thermal stratification will allow the right temperature gradient to be achieved.

4.2.2 Losses through the insulated tank

As explained in the previous sections, the losses through the casing are evaluated with formulas (16) and (17) according to the conditions inside and outside the tank.

For this study, it was assumed that the tank was installed on a ground support, in the Milan area, where the average annual temperature is about $13°C$.

On the following pages, Table 6 shows the result of the calculations performed, in which the limiting coefficient of water was obtained from (Calza, 2010, p. 126).

Wall stratigraphy			
Layer	*Thickness*	*Conductivity*	*Transmittance*
	m	*W/mK*	*W/m²K*
External conductive coefficient	//	//	25.00
Stiferite GT	0.1	0.023	0.23
Stiferite GT	0.1	0.023	0.23
CLS concrete	0.1	1.600	16.00
Vertical wall (air/air)			
Internal conductive coefficient		W/m²K	8.00
Total thermal transmittance		W/m²K	0.11
Total surface		m²	19.02
Horizontal wall – Ascending flux (air/air)			
Internal conductive coefficient		W/m²K	9.30
Total thermal transmittance		W/m²K	0.11
Total surface		m²	21.39
Vertical wall (air/water)			
Internal conductive coefficient		W/m²K	800.00
Total thermal transmittance		W/m²K	0.11
Total surface		m²	34.80
Ground dispersion			

Ground type	type	sand/gravel
Ground conductivity	W/mK	2.00
Heat capacity per unit of volume	kJ/m³K	2000.00
Specific size (area / perimeter)	m	1.84
Total thickness of external perimeter walls	m	0.30
Internal surface thermal resistance	m²K/W	0.0013
Equivalent thickness	m	0.38
Thermal transmittance	W/m²K	1.80
Total surface	m²	21.39
Power losses from the tank		
Average annual outdoor temperature (Milan, Italy)	°C	13.00
Average internal temperature	°C	35.00
Power loss	**kW**	**1.03**

Table 6. Power loss from the tank

4.2.3 Evaporated flow rate

The determination of the amount of evaporating water represents a fundamental point of the process, primarily because knowing this allows us to establish the maximum value of condensate that we can obtain in the conditions the plant is working in, and secondly because in this way we can also evaluate the flow rate of salt water to be reintegrated into the system. The total evaporating surface is divided in half by the presence of the thermal tunnel, both halves operating under the same operating conditions; this allowed us to perform the calculation on one of the two halves of the tank and then extend it to the entire evaporating surface.
Table 7 shows the results obtained from the application of the model:

Physical state of water on the free surface		
Hygrometric degree	//	1.00
Saturation pressure	Pa	19,943.76
Partial vapour pressure	Pa	19,943.76
Physical state of dehumidified water		
Kinematic viscosity	m²/s	0.0000162
Hygrometric degree	//	1.00
Saturation pressure	Pa	4246.03
Partial vapour pressure	Pa	4246.03
Other data		
Specific size	m	0.90
Universal constant of perfect gases	J/kmolK	8314.00
Molar mass of water	kg/kmol	18.00
Binary diffusion at the process conditions	m²/s	0.0000974
Adimensional number		

Reynolds	//	500,000.00
Schmidt	//	0.17
Sherwood (laminar flux)	//	258.23
Evaporated water flow		
Conveying material transport coefficient	m/s	0.0279
Flow of water evaporated from one half of the tank	kg/s	0.0232
Total evaporated water flow	**kg/s**	**0.0464**
	kg/d	**4012.09**

<div align="center">Table 7. Total water flow</div>

Table 8 shows the calculation of the power transmitted to the air through latent heat:

Latent heat of vaporization at operating conditions	kJ/kg	2362.37
Thermal power transferred	**kW**	**109.70**

<div align="center">Table 8. Power transferred during evaporation</div>

The thermophysical parameters used in Table 7 have been obtained from tables showing the properties of air (Moran et al., 2011; Magrini & Magnani, 2009).

The value of the binary diffusivity was obtained from suitable diagrams in conditions of pressure and temperature equal to $1\ atm$ and $300\ K$; to bring it back to the process conditions, the following formula was applied, remembering that the binary diffusivity of the perfect gases is approximately proportional to the relation:

$$D_{AB} = D_{AB(300K;1atm)}\left(\frac{P}{P_{ex}}\right)\left(\frac{T_{ex}}{T}\right)^{1,75} \qquad \left[\frac{m^2}{s}\right] \qquad (26)$$

where P_{ex} and T_{ex} represent the pressure and operating temperature, expressed in atmospheres and Kelvin (Subramanian, p. 1).

The value of the latent heat was evaluated at the working pressure through the aforementioned tables; in order to bring it back to the temperature conditions of the system, the Watson correlation was exploited (Pantani, 2010, p. 10):

$$r_{p,t_{ex}} = r_{p_{ex}}\left(\frac{T_c - T_{ex}}{T_c - T_{eb}}\right)^{0,38} \qquad \left[\frac{kJ}{kg}\right] \qquad (27)$$

where:
- $r_{p_{ex}}[kJ/kg]$: latent heat of vaporization at working pressure;
- $T_c[K]$: critical temperature, equal to $647\ K$;
- $T_{eb}[K]$: boiling temperature at operating pressure conditions, equal to $342.25\ K\ (69.1°C)$.

With the conditions of speed, pressure and temperature adopted, it is possible to push the system up to a daily production of approximately $4000\ kg/d$ of evaporated water. This will be the maximum condensable amount in the system.

The peculiarity of this process lies in the possibility of fully recovering the latent heat of vaporization, quantified in a power value of approximately $110.00\ kW$.

4.2.4 Primary heat exchanger

The main heat exchanger performs a triple function:
- It transmits the thermal energy necessary to raise the salt water temperature near the free surface from its initial value up to the process temperature;
- It transmits the thermal energy needed to replenish leaks through the enclosure, helping to keep the temperature at the operating level;
- Through an adequate control of the delivery and return temperatures, it creates a thermal gradient between the central area near the thermal tunnel and the side walls of the casing; this configuration allows the

majority of the evaporated water to be concentrated in the area closest to the expanded sheets, promoting the rotation of convective motions in the right direction.

As stated in paragraph 4.1.3, the use of corrugated pipes has been chosen, firstly because they promote the turbulent motion, thus increasing the convective heat exchange coefficient and the amount of energy transmissible per unit of length, and secondly because it is thought that the turbulent motion creates micro-vibrations which, when transmitted to the salt water at the free surface, promote its evaporation.

The preliminary evaluation of the heat exchange was performed by putting in conservative conditions and carrying out the calculation assuming the use of a smooth tube. In the tank there will be two exchangers of this type, one placed in each half of the tank, and both return flow connections will be connected to the heat generators through two suitable hydraulic manifolds.

Table 9 shows the summary of the calculations:

Operating temperature		
Delivery temperature	°C	75.00
Return temperature	°C	45.00
Piping		
Outer diameter	mm	32.00
Thickness	mm	1.50
Internal diameter	mm	29.00
Operating data		
Internal speed to the pipes	m/s	1.50
Fresh water density	kg/m³	1000.00
Fresh water specific heat	kJ/kgK	4.186
Flow		
Volumetric flow rate exchanger - half tank	m³/h	3.57
Total volumetric flow	m³/h	7.13
Heat exchanger (half tank)		
Step (distance between two contiguous hole centres)	m/MU	0.082
Number of passes approximated down	MU	10.00
Estimated pipe length	m	93.00
Power transmissible		
Thermal power transmissible from the single exchanger	**kW**	**124.42**

Table 9. Primary heat exchanger sizing

To ensure that the correct transversal temperature gradient is present in the tank, it is decided to perform the control monitoring of the temperature of the return fluid to the system; once this reaches the preset value, knowing that of the delivery temperature, the sending of thermal energy can be stopped.

4.2.5 Condensate production

The evaluation of the production of condensate must take into account the fact that it is subordinate to the quantity of evaporating water. As explained previously, in the best operating conditions the maximum amount of condensable water will be equal to the maximum evaporating quantity; it will therefore be necessary to size the thermal tunnel condenser in such a way as to allow condensation of this quantity of water.

To calculate the amount of condensate produced, it is necessary to know the thermo-hygrometric conditions of the humid air inside the tank before and after condensation and to know the dry air flow to determine the sizing power of the exchangers. Table 10 shows the results of applying the model:

Hygrometric condition		
Specificy humidity - humidified air	g_v/kg_{as}	1240.00
Specific humidity - dehumidified air	g_v/kg_{as}	102.80
Condensate production		
Amount of specific condensate	g_v/kg_{as}	1137.20
Air flow needed		
Mass flow of dry air	kg/s	0.04
	kg/h	147.00
Partial pressure of dry air	Pa	10,056.24
Dry air specific constant	J/kgK	287.00
Mass flow of moist air	kg/s	0.39
	kg/h	1397.05
Condensing power		
Enthalpy moist air - humidified air	kJ/kg	3300.00
Enthalpy moist air - dehumidified air	kJ/kg	293.00
Enthalpy of condensed	kJ/kg	125.79
Condensation power	**kW**	**-116.95**

Table 10. Condensing power

To be able to condense the same amount of water that evaporates, it is necessary to create an exchange surface that allows the absorption of a thermal power equal to $116.95\,kW$. This must be ensured through a suitable sizing of the stretched sheets of the thermal tunnel. As can be seen, the resulting power is slightly higher than that calculated for the evaporation, because it also considers the enthalpy contained in the condensate and not only that of the humid air to the initial and final states of the transformation.

4.2.6 Condensation support - expanded sheets

The thermal power necessary to be able to condense the same flow of water that evaporates must be absorbed by a suitable heat exchanger, which in our case has a double function:
- It enables heat exchange and disposal of the large amount of energy transferred during the condensation phase;
- It allows the condensed water to percolate above it up to a collecting channel.

In addition to having the proper thermal properties to be used for the purpose, therefore, it must also have mechanical characteristics such as to make it an excellent support on which the condensed water can adhere.

The disposition of the expanded metal sheets must be made in such a way as to minimize the interference between adjacent sheets, maximizing the interaction between the fluid and the exchange surface. Moreover, the opening of the expanded metal sheets in the upper part of the system must be made in such a way that the minimum inclination of the plate with respect to the horizontal enables the adhesion forces to allow the condensate drop to adhere to the metal surface and to percolate towards the collection system, avoiding it falling into the tank. The mathematical modelling of these aspects requires complex analyses in the field of microfluidics, since the common calculation models that analyse macroscopic phenomena are not representative. For the preliminary dimensioning, it was preferred to obtain the value of the maximum inclination angle experimentally, observing the behaviour of a drop of water in contact with an aluminum surface inclined with ever increasing slopes. The result shows that, to ensure the rapid disposal of condensate drops, preventing them from being detached, the outer sheets must form an angle of no less than approximately 50°C. Below this value it has been observed that the drop speed of the drops decreases, causing an increase of mass and the consequent detachment from the contact surface.

Table 11 shows the results of the application of the calculation method reported in paragraph 3.1.3.4:

Presumed temperature at the base of the thermal tunnel	°C	20.00
Convective coefficient at the base of the tunnel	W/m²K	3149.20
Reduction hypothesis due to the insulating overlap	%	30.00%
Presumptive convective coefficient	W/m²K	944.76
Thermal conductivity of aluminum	W/mK	210.00
Expanded metal commercial surface	m²	2.00
Equivalent metal surface	m²	1.54
Fin length	m	0.80
"m" coefficient of the fin	1/m	67.07
"A" coefficient of the fin	K	-40.00
"B" coefficient of the fin	K	0.00
Specific thermal flow	kW/fin	-0.90
Number of fins	**fin**	**15.00**

Table 11. Thermal tunnel sizing

The base of the thermal tunnel is a region with high thermal conductivity and is in direct contact with the colder water at the bottom of the tank. Therefore, its temperature has been hypothesized not to be much higher than that at the bottom. In order to avoid the heat developed by the main heat exchanger being transmitted to the expanded sheets, disturbing the absorption of thermal energy during condensation, the insulation panels of the thermal tunnel will be extended beyond the base for a certain length, which will be established during the project execution. This extension is thought to lead to a significant reduction in the convective heat exchange coefficient between the base of the thermal tunnel and the air to be dehumidified. Therefore, to consider this phenomenon, a reduction of 30% was considered.

The expanded metal will exit the base of the thermal tunnel for a length equal to $80\ cm$, and the remaining part will pass through the thermal tunnel and will be immersed in the coldest salt water at the bottom of the tank.

The number of rows has been evaluated assuming the support of nine stretched sheets to form an extension having a length equal to $9\ m$. For compatibility with the capacity of the industrial processes available, in the executive design phase we will evaluate, together with the manufacturing companies, the best method to join the sheets.

4.2.7 Heat generation

As explained in the previous section, the SDGC system is designed to be able to self-maintain when brought to operating temperatures. For this purpose, it was decided to use two different heat generators:
- Solar thermal system: this operates mainly under the regime conditions in order to reintegrate the heat losses through the enclosure;
- Heat pump system: this operates mainly at start-up, in order to bring salt water from the feed from the conditions in the tank up to the average operating temperature.

However, while the two plants can work in synergy to reduce the start-up times, solar thermal will be the primary generator once the SDGC system has reached full capacity.

4.2.7.1 Solar thermal generator

For the case study, the use of vacuum solar collectors was chosen because of their ability to bring the water to high temperatures, in harmony with those of operating the plant. The type of collector chosen for sizing is the Sky Pro 18 model produced by the company Kloben Industries S.r.l, having the characteristics of interest shown in Table 12:

Optical efficiency	%	71.80%
Opening surface	m²	3.43
Absorption surface	m²	4.65

Heat loss - 1st order	W/m²K	1.051
Heat loss - 2nd order	W/m²K	0.004

Table 12. Kloben Sky Pro 18

The sizing of the collectors was carried out assuming installation of the plant in Milan and considering the operating system for $8000 h/year$.

To obtain a datum concerning the minimum number of collectors necessary, it was decided to calculate the global radiation assuming installation of the collector in the best possible operating conditions, which translates into:

• Geographic orientation in the SOUTH direction (azimuth equal to $0°$);
• Angle of inclination on the horizontal optimal for the operation of solar panels (35°);
• Absence of shadowing and obstacles.

Under these assumptions, the operational efficiency of the collector was calculated using the following formula (Battisti, 2013, p. 17):

$$\eta = \eta_o - \frac{k_1}{I}\Delta T - \frac{k_2}{I}\Delta T^2 \qquad [\%] \qquad (28)$$

in which:

• $\eta_o[\%]$: optical efficiency of the collector. This represents the amount of solar radiation reflected on the collector's opening surface that can be transformed into useful thermal energy, calculated under certain measurement conditions.
• $k_1,k_2[W/m^2K]$: thermal dispersion coefficients. These quantify the amount of thermal energy lost by conduction through the collector material, thermal radiation and convection.
• $\Delta T[Ko°C]$: difference between the average temperature inside the collector and the external environment;
• $I[W/m^2]$: effective irradiation on the collector.

Once the operating efficiency of the collector had been calculated, the radiation actually transmitted to the water from the collectors was evaluated and from this the necessary surface was found for the heat exchange to take place.

Finally, the number of collectors needed was calculated; as a characteristic datum for the calculation, the opening surface is used more and more, but also the absorption surface is taken into consideration. In the calculations it is therefore essential to discriminate the source of the results according to the two surfaces considered. In the case study, the number of collectors was evaluated using both surfaces and choosing the one with the largest number of collectors. Table 13 shows the results of the calculations performed:

Energy losses from the tank		
Hours of operation per year	h/year	8000.00
Annual energy loss	kWh/year	8276.80
Solar radiation on inclined surface		
Location	//	Milan
Azimuth	°	0.00
Inclination with respect to the horizontal plane	°	35.00
Reflection coefficient on the ground	//	0.20
Shadows and obstacles	//	none
Global radiation on inclined surface	kWh/m²year	1612.00
Irradiation on inclined surface	W/m²	184.02
Solar collectors operating efficency		
Thermal medium fluid temperature	°C	60.00
Average annual room temperature	°C	13.00

Collector operational efficiency	%	40.15%
Solar collectors numbers		
Effective radiation absorbed by the collector	kWh/m²year	647.29
Exchange surface required	m²	12.79
Number of collectors - opening surface	//	4.00
Number of collectors - absorption surface	//	3.00
Numbers of solar collectors	**//**	**4.00**

Table 13. Solar collectors sizing

Therefore, the minimum number of collectors required, calculated in the best operating conditions, is four.

4.2.7.2 Heat pump generator

To allow rapid achievement of the expected operating conditions, it was considered appropriate to assist the solar thermal system through the use of a second heat generator. Among the various choices available on the market, the one that most reflects the need to have an efficient and low environmental impact energy source is heat pump technology.

In a first evaluation it was decided to couple the heat pump to a suitably sized geothermal probe system. However, the costs for the geological analyses and, above all, for the drilling of the ground and the installation of the probes did not justify the use of the machine. As explained in the previous pages, in fact, we want the heat pump to run at full capacity only during start-ups which, for the good functioning of the system, we want to reduce to the minimum number needed. From this it is easy to understand that investing excessive resources for a technology that will be used very sporadically is uneconomic.

For the case study it was therefore decided to use a water / water heat pump, in which the evaporator is in communication with a thermocouple.

Introduction to the thermal flywheel: this system consists of an artificial waterproof well with a volume of a few tens of cubic meters, capable of accumulating the thermal energy of the superficial layers of the ground, also acting as a thermal flywheel to store the excess heat produced, for example, from a solar collector. This system, which will be integrated in the future development of the SDGC system, allows the storage and exploitation of the heat of the ground at reasonable costs compared to the more expensive geothermal probes (Lavanga & Sparacino, Termopozzo, 2013).

The calculations for the case study were made taking into account the Vitocal 300-G heat pump, model WW 301.A21, produced by the company Viessmann GmbH. This machine is able to operate both as a ground / water heat pump and as a water / water heat pump. Table 14 shows the main operating data:

Performance data - EN 14511		
Operating conditions	//	W10/W35
Useful power	kW	28.10
Refrigeration power	kW	23.70
Electric power absorbed	kW	4.73
Performance coefficient (COP)	//	5.94
Primary circuit (evaporator)		
Capacity	l	6.50
Minimum volumetric flow rate	l/h	5200.00
Loss of load	kPa	17.00
Maximum flow temperature (ground circuit input)	°C	25.00
Minimum flow temperature (ground circuit input)	°C	7.50
Secondary circuit (condenser)		

Capacity	l	6.50
Minimum volumetric flow rate	l/h	1900.00
Loss of load	kPa	3.80
Maximum flow temperature	°C	60.00

Table 14. Vitocal 300-G datasheet

For a first analysis we chose to operate conditions $W10/W55$. In this way the salt water will be brought to the temperature of $55°C$ and the solar thermal plant will be responsible for compensating the small temperature difference between the heat pump regime and the average operating temperature. It was decided to operate in this way to avoid a too high penalty on the COP. Table 15 shows the results of the calculations performed:

Energy requirements		
Salt water temperature at the entrance	°C	15.00
Operating temperature for heat pump	°C	55.00
Specific salt water heat	kJ/kgK	3.93
Salt water density	kg/m³	1025.00
Mass to be heated	kg	5147.55
Thermal energy to be supplied	**kWh**	**224.49**
Heat pump - operating conditions		
Thermal power yield	kW	24.92
Performance coefficient (COP)	//	3.68
Electric power absorbed	kW	6.77
Hours of operation		
Time needed to go to full capacity	**h**	**9.01**

Table 15. Vitocal 300-G - operating contitions

In the calculation, the volume (and consequently the mass) of salt water to be heated was considered equal to 30% of the whole salt water mass inside the tank, again because the objective is to heat only the portion of fluid near the free surface.

The results show that, in those operating conditions, for the plant to be able to operate through only the thermal energy provided by the solar plant will take just over $9h$, which is a decidedly good start time. Figure 14 shows a diagram of the layout of the SDGC plant with heat generators.
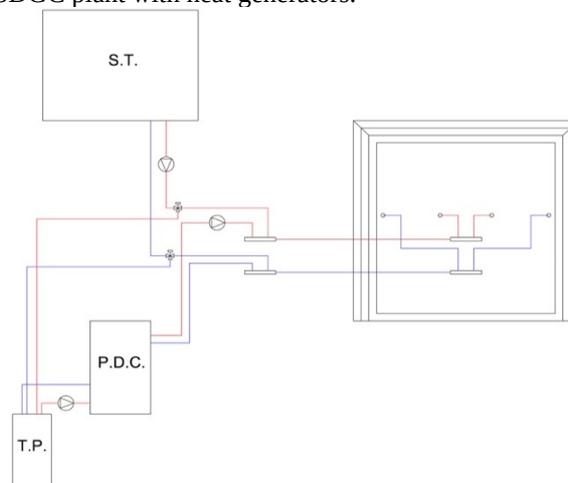

Figure 14. SDGC simplified plant layout

4.2.8 Critical functioning

Despite its simple construction, the system is not exempt from possible anomalies. The operation is based on the rigid maintenance of well-defined thermal gradients; in the absence of such temperature differences, the system can drastically reduce the production of condensation up to the complete shutdown of the system.

The worst condition is reached when the thermal gradients are reset and the tank is all at the same temperature; in this case, the evaporation stops (due to having the same saturation pressure at each point) and the heat cannot circulate through the thermal tunnel.

In this case it is necessary to break the thermal equilibrium, re-establishing the right gradients so that the system resumes operation. To this end, auxiliary safety exchangers are installed that can transfer the thermal energy from one area of the tank to another or transfer it to the thermocouple in the event of excess. These exchangers must be able to restart the system as soon as possible, so they must be able to transfer a large amount of heat in a short time.

4.2.8.1 Upper / lower heat exchangers

The thermal tunnel represents a possible bottleneck for the plant. This element, in fact, must guarantee the passage of all the thermal energy absorbed by the expanded sheets during the condensation process; if this function could not be carried out efficiently, these would gradually increase to the same temperature as the humid air, thus slowing down the process until it stopped.

To compensate for this drawback, in the first analysis it was assumed to install a piping circuit (again made of corrugated material) passing between the upper and lower part of the tank, filled with a heat-carrying fluid (water or other better performing fluids). With the aid of a hydraulic pump, the movement of the fluid would allow the absorption of thermal energy from the humidified air to transfer it to the colder water at the bottom of the tank. In this way, the thermal tunnel would be able to dispose of the remaining thermal energy without the risk of reaching the thermal equilibrium between the humidified air and expanded sheets.

The dimensioning of these pipes was carried out in the light of the fact that, should the need arise, this exchanger must be able to absorb a large amount of thermal energy in a short time. The calculation shown in Table 16 follows the calculation principles dictated by technical physics (Magrini & Magnani, 2009, p. 173), in which some parameters have been set:

- The temperature of the thermal fluid inlet and outlet from the pipeline, on which the thermophysical parameters necessary for the calculation depend;
- The dimensions and material of the piping, referred to standardized industrial products.
- The internal speed in the piping;

The calculation provided for the determination of the conductive and convective thermal resistance (internal and external side) of the piping, for which it was necessary to calculate the convective heat exchange coefficients on the inside and outside according to the commonly used calculation models (Moran et al., 2011; Magrini & Magnani, 2009). The dimensioning of the exchanger was carried out considering the exchange with air. Achieving a satisfactory degree of absorption in this area, we are sure that this will be just as good for the salt water exchange zone, by virtue of its greater thermal conductivity. Furthermore, even for this exchanger the calculation was conservative.

Fresh water data		
Delivery temperature	°C	20.00
Minimum return temperature	°C	50.00
Average temperature	°C	35.00
Thermal conductivity at average temperature	W/mK	0.62
Kinematic viscosity at average temperature	m^2/s	7.52E-07
Piping data		
Estimated length	m	9.30
Outer diameter	mm	50.00
Thickness	mm	1.00
Internal fluid speed	m/s	2.50
Material conductivity	W/mK	390.00

Conductive resistance	K/W	1.79E-06

Internal convective heat resistance		
Prandtl	//	5.04
Reynolds	//	159,574.47
Nusselt - turbulent flux in heating	//	638.57
Internal convective coefficient	W/m^{2}K	8242.88
Internal convective heat resistance	K/W	8.65E-05

External convective heat resistance		
Film temperature	K	320.5
Kinematic air viscosity at the film temperature	m^2/s	1.77E-05
Thermal conductivity at the film temperature	W/mK	0.02754
Reynolds	//	25,359.26
Prandtl	//	0.7099
Nusselt - laminar flow	//	102.0706701
External convective coefficient	W/m^{2}K	56.22
External convective thermal resistance	K/W	1.22E-02

Power		
Total thermal resistance	K/W	1.23E-02
Thermal power absorbed	**kW**	**3.26**
Number of installations	exchangers	15.00
Potential for total exchange	**kW**	**48.92**

Table 16. Secondary heat exchanger (upper/lower)

By installing 15 pipes connected in parallel through a suitable collector, the system is able to absorb a quantity of heat equal to about 40% of the total to be disposed of through the thermal tunnel, enough to restart the process in the event of a system stall.

4.2.8.2 Side heat exchangers

As stated in the previous pages, the worst criticality for the operation of the system is represented by the zeroing of the thermal gradients. This situation can occur for two main reasons:
- In the system, insufficient thermal energy was introduced to compensate for losses through the enclosure and to guarantee the formation of thermal gradients suitable for making the system work efficiently.
- Too much thermal energy was introduced into the system, saturating the system and bringing the tank to the same temperature at each point.

While in the first case it is sufficient to introduce further thermal energy, the second case certainly deserves more attention. It may be due to malfunctions or to unsuitable control systems. In any case, if this situation occurs, the tank being well insulated and therefore with limited losses, it is necessary to withdraw a portion of this thermal energy and transfer it outside the system in order to restore the thermal gradients necessary to restart the process. For this purpose, it was decided to install a series of pipes along the side walls of the tank, similar to the solution adopted in the previous paragraph, in which a heat-carrying fluid is circulated to absorb thermal energy from the salt water and transport it outwards, to be dissipated in the environment or stored in a thermal storage system. In this way, the cooling of the salt water will allow the thermal tunnel to start the condensation process again. Table 17 shows the calculations performed for sizing, which require the selection of some parameters, as explained in paragraph 4.2.8.1.

Fresh water data		

Delivery temperature	°C	20.00
Minimum return temperature	°C	50.00
Average temperature	°C	35.00
Thermal conductivity at average temperature	W/mK	0.62
Kinematic viscosity at average temperature	m²/s	7.52E-07
Piping data		
Estimated length	m	18.60
Outer diameter	mm	50.00
Thickness	mm	1.00
Internal fluid speed	m/s	2.50
Thermal conductivity	W/mK	390.00
Conductive resistance	K/W	8.96E-07
Internal convective heat resistance		
Prandtl	//	5.04
Reynolds	//	159,574.47
Nusselt - turbulent flux	//	638.57
Internal convective coefficient	W/m²K	8242.88
Internal convective heat resistance	K/W	4.33E-05
External convective heat resistance		
Film temperature	K	320.50
Kinematic air viscosity at the film temperature	m²/s	5.86E-07
Thermal conductivity at the film temperature	W/mK	0.64
Cubic expansion coefficient	1/K	4.37E-04
Grashoff	//	3.90E+07
Prandtl	//	3.76
Rayleigh	//	1.47E+08
Nusselt	//	76.48
External convective coefficient	W/m²K	975.20
External convective thermal resistance	K/W	3.51E-04
Power		
Total thermal resistance	K/W	3.95E-04
Thermal power absorbed	**kW**	**63.27**
Number of installations	exchangers	6.00
Potential for total exchange	**kW**	**379.63**

Table 17. Secondary heat exchanger (left/right)

By installing six exchangers in parallel close to the sidewalls of the tank, they will be able to absorb about 380 kW of thermal power. This power will be sufficient to break the thermal equilibrium by bringing the system to work again in a time of about $3\ h$. Table 18 gives a verification calculation.

Balance temperature	°C	60.00
Operating recovery temperature	°C	20.00
Total mass of water	kg	33,617.95
Mass of water to be cooled	kg	23,532.57
Energy spent on cooling	MJ	3940.29
	MWh	1.09
Time spent cooling	**h**	**2.88**

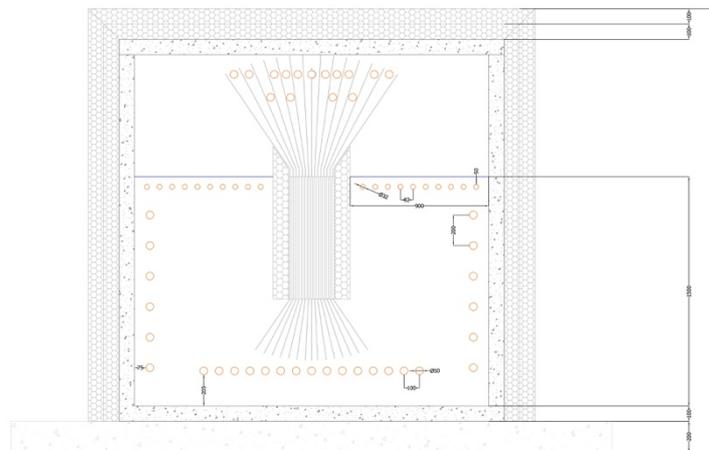Table 18. Secondary heat exchanger - validation

Figure 15. SDGC heat exchangers simplified layout

Once the sizing of the main elements of the system has been completed, Figure 15 shows the dimensioned drawing of the SDGC system.

4.2.9 Auxiliary plants

For the good functioning of the system it is necessary that the tank remains closed most of the time, allocating the opening and therefore the shutdown of the system only in case of scheduled maintenance or in cases of overtime. This makes it necessary to design a series of auxiliary service systems able to maintain the adiabatic tendency of the tank, the vacuum of the tank and at the same time guarantee the continuity of the process.
The plants covered by this paragraph are:
- Brine removal plant;
- Salt water intake system;
- Condensate extraction system;
- Control and regulation system.
- Vacuum system of the tank.

The study and design of these plant portions will be the subject of future developments of the SDGC system. The following is a construction concept in order to justify the purchase and installation costs reported in the economic analysis of the next section.

4.2.9.1 Brine removal system

During the process of the evaporation of salt water, the chemical reaction of the separation of water from the salts takes place, as reported in paragraph 2.2. As a result of this separation, during the process the salt water that remains inside the tank will be increasingly enriched in salts, increasing their concentration up to a maximum limit beyond which the water will no longer be able to dissolve them, causing them to sink to the bottom of the tank.

To guarantee the efficient removal of the brine (where this term refers to salt water which has undergone a partial increase in the concentration in salts), it will be necessary to provide for its partial replacement with a reintegration of salt water before the limit of concentration.

For a first evaluation it was decided to arrange, homogeneously on the bottom of the tank, a perforated pipe connected to a hydraulic pump able to effectively suck out the brine deposited on the bottom. The machine can be connected to a level sensor, which measures the position of the free surface when it falls below a certain value, or to a sensor that detects the degree of concentration of salts in the solution.

4.2.9.2 Salt water intake system

During operation and as stated in the previous paragraph, the water evaporation process and the brine removal must correspond to a simultaneous reintegration of the salt water, in order to maintain the level of the free surface above the pipes of the main heat exchanger. This operation can be carried out simply by connecting a pipe to one or more nozzles located on the side walls of the tank and connected to a hydraulic pump connected to an external storage tank that guarantees a certain autonomy. The system must also be able to provide rapid filling of the tank during start-up or at the end of scheduled maintenance.

4.2.9.3 Condensate extraction system

The water is condensed by the cooling process. To avoid this energy being dissipated in the external environment, a possible solution that will be the subject of future work could be to preheat the salt water using energy contained in the condensate. To accomplish this, double-walled piping could be used to inject salt water into the tank, so that the condensate during the outlet travels through the innermost pipeline, yielding thermal energy to the salt water entering through the outer piping. To collect the condensate, a possible evaluated solution consists in the installation of a collection tank at the base of the thermal tunnel with a certain slope, so as to allow the condensate to exit from the gravity tank until it flows into an external tank. From there, a hydraulic pump would send it for the final use through the double-walled pipe described above.

4.2.9.4 Control and regulation system

Monitoring and control of the system parameters is the nerve point of the whole system. As explained in the previous sections, good operation is based on the strict maintenance of thermal gradients and established operating conditions. This can only be achieved if upstream there is an effective control system that allows the total management of the entire system, from heat generators to safety exchangers, until you get to the reintegration of the salt water and to maintaining the speed of the indoor air. All this can be achieved through a series of appropriate sensors. Pressure, level, temperature, velocity, concentration and weather sensors to manage the solar thermal system are just some of the possible devices that can be used by the system to work properly.

4.2.9.5 Vacuum system for the tank

Natural water evaporation is a rather slow process. Think of an open container filled with water and left in the environment; a few hours will pass before it empties. To speed up this transformation we can use different strategies, all exploited within the SDGC system: air acceleration in order to promote convective motions, increase of the water temperature to increase molecular agitation and promote diffusion, and finally vacuuming the environment in which the water must evaporate. By reducing the total pressure inside the tank, evaporation is greatly facilitated; as shown by formula (8), decreasing the value of the total pressure increases the value of the natural logarithm and, consequently, the molar flow of evaporated water.

To evacuate a container, it is necessary to establish a pressure difference between the container to be emptied and another region of space. To obtain this condition, vacuum pumps are used, suction devices capable of emptying closed containers containing liquids, sucking out part of the air inside. The suction system of the tank must be able to maintain the degree of vacuum expected during the sizing phase for a sufficiently long time not to require continuous operation of the machine. For this reason, it will be necessary to provide adequate sealing systems both for the air extraction system and for the connections of the other auxiliary systems for the entry and removal of salt water and for the extraction of condensation.

Economic analysis

This section presents the results derived from the use of the SDGC system as a desalination system. The analysis was carried out taking into account the main costs and making an estimate for all the elements that, at present, have not yet been designed in detail. All this makes it possible to derive a first evaluation of the costs connected to the construction and operation of the plant during the prototyping phase and allows a first comparison to be made with existing technologies. The cost analysis was performed considering the cost of the SDGC module only, without considering any pre-treatment systems for salt water or post-treatment of fresh water.

It is recalled that the standard module of the previous sizing can easily be replicated in parallel to cover the required fresh water requirement. Thanks to scale effects and design revaluation on auxiliary and generating systems, as the production size increases, the cost of specific plants will decrease considerably.

5.1 Cost of plant

The cost of the plant represents the total costs incurred for its construction. The total represents the initial capital needed for the plant to be ready to produce. Table 19 shows the evaluation of the plant cost, considering the materials needed and the implementation of a single SDGC module.

Description of cost items	Price [€]
Reinforced concrete tank 53 m^3	7000.00
Insulation panel 100 mm	3840.00
Corrugated tube CU 32x1.5 mm	1674.00
Corrugated tube CU 50x1 mm	5070.00
Rhomboidal expanded sheet Al 62x20 sp.2 vp.30%	6750.00
Solar collectors Sky Pro 18 + Mechanical support	4000.00
Heat pump W/W 301.A21	7000.00
Auxiliary plants - machines - control and regulation systems	6000.00
Civil works (foundation + machine room)	5000.00
Installation - total workforce	7000.00
Total	**53,334.00**

Table 19. Unit module cost

The table shows that the implementation of the system involves an estimated initial outlay of about 53,000.00€, which for the current level of development can be considered sufficiently reliable based on the fact that the materials used in the construction are all standardized products used in the industrial sector.

5.2 Operating cost

The operating cost represents the sum of all the costs to be incurred in a given period (the year is considered) to operate the plant correctly, so as to maintain its performance characteristics at the project conditions.

At present, the operating cost of the SDGC system represents a difficult point of analysis, since there is not yet a prototype that allows reference values to be considered. The determination, therefore, was carried out on the basis of a careful critical analysis of the operation over the reference period, assuming what could be the possible costs to be taken into account and to what extent. The operating costs considered in the calculation are shown below:

- Management: the system has been designed to be able to operate autonomously through an appropriate control and regulation system, not requiring the presence of permanent personnel. In this first phase it is considered opportune that the system can be monitored remotely, even if, as we will see below, as the size increases, it may be more convenient to hire staff.
- Electricity: at present, the possibility of installing a photovoltaic system capable of supplying the total amount of electricity required has not yet been assessed, therefore the connection to the electricity grid is assumed with a contract at an industrial price. For the reasons stated above, the evaluation of the electrical consumption of the plant is difficult to determine; for a first analysis it was assumed to set the utilization coefficients that would allow an estimate of the number of equivalent operating hours on the total shown in Table 20.
- Ordinary maintenance: scheduled maintenance interventions are expected to be limited to cleaning the tank from possible encrustations and, where necessary, to the treatment of the elements in contact with salt water with anti-corrosion products.

Table 21 shows the estimated costs necessary to maintain the SDGC system in the operating conditions established in the design phase.

Factor of use of main pumps	0.2	The pump serving the solar thermal system works for approximately 1600 h/year equivalent.
Use of secondary / auxiliary pumps	0.013	The pumps serving the safety and in / out salt water systems work for approximately 104 h/year equivalent.
Heat pump utilization factor	0.01	The heat pump works for around 80 h/year equivalent.

Table 20. Unit module operating cost

Global data		
Annual operation	h/year	8000.00
Industrial electricity price	€/kWh	0.12
Rated power for solar thermal pumps	kW	0.75
Rated power for auxiliary pumps	kW	1.10
Estimated energy consumption		
Heat pump energy consumption	kWh/year	541.74
Solar thermal pump energy consumption	kWh/year	1200.00
Power consumption of auxiliary pumps	kWh/year	686.40
Total electricity consumption	kWh/year	2428.14
Operating cost		
Electric energy	€/year	291.38
Routine maintenance	€/year	550.00
Remote management contract	€/year	1000.00
Total	**€/year**	**1841.38**

Table 21. Electric power usage factors

From a first estimate it is therefore clear that the order of magnitude of the annual operating costs of a unit can be evaluated as approximately 1800.00 €/$year$.

5.3 Production cost

From what has been described in the previous paragraphs, it is possible to evaluate a first estimate of the production cost of desalinated water through the SDGC system. By fixing the operating period of the system as 8000 $h/year$, it is possible to obtain the quantity of water produced through an SDGC module. By dividing this amount by the operating costs, the unit production cost of desalinated water is obtained. Table 22 shows the results.

Annual production of desalinated water	m³/year	1337.36
Specific consumption	kWh/m³	1.82
Specific production cost	**€/m³**	**1.38**

Table 22. Fresh water specific production cost

Therefore, for an SDGC plant made up of only one operating module, the specific cost of producing desalinated water is equal to 1.38 €/m^3 compared to an energy consumption of 1.82 kWh/m^3.

Please note that this cost has been assessed without considering any contributions due to the operation of water treatment systems, which may be necessary in relation to the occurrence of particular conditions of the supply water (presence of disturbing elements that could clog or damage hydraulic machines at the service of the plant) or in relation to the particular use of desalinated water. Moreover, the easy modularity of the plant allows its production to be increased against a less than proportional increase in operating costs.

5.4 Comparison with existing technologies

The following section shows a comparison, in terms of distillate production and specific consumption, between the SDGC plant and the existing technologies supplied with traditional sources. In Table 23, a first comparison can be made (de la Cruz & Cynthia, 2015):

Technology		Typical capacity	Specific consumption		Cost
		m^3/d	kWh_e/m^3	kWh_t/m^3	$€/m^3$
Processes of renewable sources	Solar still	< 0.1	//	//	1 − 6
	Solar MEH	1 − 100	1.5	100	2 − 6
	Solar MD	0.15 − 10	//	150 − 200	8 − 15
	Solar MED	> 5000	1.4 − 2	60 − 70	1.8 − 2.2
	PV-RO	< 100	0.5 − 1.5	//	5 − 7
	PV-EDR	< 100	3 − 4	//	8 − 9
	WIND - RO	50 − 2000	0.5 − 5	//	3 − 7
Conventional sources processes	MSF	6 − 500	3 − 5	70 − 90	1 - 4
	MED	10 − 200	2 − 4	70 − 90	3 − 10
	RO	10 − 120	3 − 5	//	3 − 7
SDGC		**> 4**	**1 − 3**	**//**	**< 3**

Table 23. Comparison between SDGC plant and existing desalination technologies

From Table 23 it can be seen that the SDGC system can compete with traditional systems by virtue of its low operating costs, exploiting the modularity of the plant and the economies of scale on materials.

5.5 Comparison with traditional technologies

At present it is very difficult to compare in detail the SDGC technology with the traditional ones, as the plant is at a stage of development that makes it difficult to quantify costs in addition to what is already reported in the previous paragraphs. However, it can be expected that the system will be more suitable for medium and low capacity applications (possibly up to $200/300 m^3/d$) given the production density that can be obtained with the current configuration.

Table 24 shows some values on the cost of desalinated water related to MSF and reverse osmosis plants. These costs were obtained by analysing the material present in the literature and extrapolating average values; in fact, they are subject to significant variation depending on the size, the place of installation and the characteristics of the water to be treated.

Process	MSF	RO
	$€/m^3$	$€/m^3$
Capital costs and plant construction	3500.00	2600.00
Operating costs	1.80	2.20
Production cost of desalinated water	1.32	1.25

Table 24. Orders of plant and operating costs, MSF and RO

From these values, which therefore represent orientations of orders of magnitude, it is possible to make a comparison assuming the construction of a plant capable of producing $150 m^3/d$ of desalinated water. To meet this production target, it is necessary to install 38 SDGC modules. For the analysis of plant and operating costs, it is assumed that, thanks to the modularity of the plant, the economies of scale on the materials allow a considerable reduction of the costs of building materials and civil works, as shown in Table 25.

Description of cost items	Price [€]
Reinforced concrete tank 53 m³	7000.00
Insulation panel 100 mm	3840.00
Corrugated tube CU 32x1.5 mm	1674.00
Corrugated tube CU 50x1 mm	5070.00
Rhomboidal expanded sheet Al 62x20 sp.2 vp.30%	6750.00
Civil works (foundations + machine room)	5000.00
Sub-total for single module	29,334.00
Scale effect	45.00%
Sub-total discounted for each module	16,133.70
Total construction and civil works for 38 SDGC modules	**613,080.60**

Table 25. Cost variation for building and civil works

As for the heat generation system, with the use of multiple SDGC modules, one might reconfigure the layout of the system to make it more efficient (for example, using a higher power generator to service more tanks and managing starting in sequence, rather than many low-power generators). This is thought likely to lead to significant economic benefits on the costs of heat generation systems, as shown in Table 26.

Description of cost items	Price [€]
Sub-total for single module	11,000.00
Scale effect	70.00%
Subtotal discounted for each module	3300.00
Total heat generators for 38 SDGC modules	**125,400.00**

Table 26. Cost variation for heat generators

As regards the auxiliary systems, the machines and the control and regulation system, it is believed that this cost cannot be reduced particularly, due to the increasing complexity of the plant and the management that generally characterize a large plant. On the other hand, as regards the cost of labour, better management of the number of technicians and workers could lead to cost savings.
Table 27 shows the result of the hypotheses made so far.

Auxiliaries plants - machines – regulation and control systems	
Description of cost items	Price [€]
Auxiliary plants - machines - control and regulation system	6000.00
Scale effect	40.00%
Subtotal discounted for each module	3600.00
Total auxiliary plants - machines - control and regulation for 38 SDGC modules	**136,800.00**
Installation	

Description of cost items	Price [€]
Installation - total workforce	8000.00
Scale effect	65.00%
Subtotal discounted for each module	2800.00
Total installation - labour for 38 SDGC modules	**106,400.00**

Table 27. Change in costs for auxiliaries, installation, labour

From these calculation estimates based on critical evaluations, the total cost of the plant can be calculated, corresponding to approximately $980,000$ €.

With regard to running costs, these can also be assessed through a critical assessment of the situation. As far as electricity costs are concerned, they can be considered essentially invariable with the size of the plant, as the energy requirement increases proportionately with the size, while a reduction of 30% of the ordinary maintenance cost can be assumed thanks to the economy of scale. As regards the cost of monitoring and management of the plant, it is possible to consider hiring a person in charge of this task, abandoning the hypothesis of remote management. Table 28 shows the summary of the calculations.

Electric energy	€/year	11,072.31
Ordinary maintenance	€/year	14,630.00
Staff (a worker)	€/year	20,000.00

Table 28. Change in operating costs

From this it is deduced that the operating cost of the plant is about $45,000.00 €/year$. From this simple analysis we can deduce that the specific cost in terms of the production of water is equal to $0.90 €/m^3$.

Table 29 shows the result of the comparison between the SDGC plant and the traditional technologies of the same dimensions shown previously in Table 24.

Process	MSF	RO	*SDGC*
Capital costs and plant construction [€]	525,000.00	390,000.00	**981,680.60**
Operating costs [€/year]	90,000.00	110,000.00	**45,702.31**
Desalinated water production cost [€/m³]	1.77	2.16	**0.90**

Table 29. Comparison of the same size of SDGC – MSF - RO

From this initial analysis, it emerges that, at the current state of development, the initial investment on the SDGC plant is much higher than traditional technologies. However, the cost of the plant can certainly be reduced given a design aimed at reducing costs and optimization, which has not yet been taken into account. Furthermore, the possibility of access to government grants or incentives, which could certainly result in a reduced charge for the client, cannot be ruled out.

From this analysis, however, it is possible to see how the use of the SDGC system leads to a significant reduction in operating costs and consequently to a reduction in the cost of producing desalinated water compared to traditional technologies.

From the data shown in Table 29 it is possible to evaluate the break-even time between the SDGC system and the traditional small-scale MSF and RO systems. The comparison is made on the basis of savings on operating costs, which, compared to the extra cost of building the plant, returns the minimum time that the SDGC plant will have to operate to repay the investment. The summary of the calculations is shown in Table 30:

Plants compared	MSF-SDGC	RO-SDGC	U.M.
Difference in operating costs	44,297.69	64,297.69	€/year
Difference with SDGC	456,680.60	591,680.60	€
Break-even time	10.31	9.20	year

Table 30. Economic analysis of SDGC - MSF - RO

As can be seen from the table, the extra cost of realizing the SDGC plant compared to the traditional ones is paid back, by virtue of lower operating costs, in a period of $9-11$ years based on the technology. Strictly speaking, in

order to evaluate the comparison between investments more precisely, cash flows should be discounted. However, the current economic situation shows that interest rates are almost zero; in a first approximation, therefore, the results obtained in Table 30 can be considered sufficiently reliable.

Considering that the average life of systems of this type is between 20 and 30 years, the use of an SDGC plant can allow a considerable economic saving starting from the break-even point of costs.

Conclusions and future developments

This document has presented the first phase of the development of the Solar Desalination Geoassisted Continuous system, a new and innovative type of system for desalinating marine waters through a rational use of energy.

In the first part of the document, the most widespread techniques used to date for the desalination of salty and brackish waters have been recalled, showing that almost all of them are operating using a large amount of energy produced using conventional sources to satisfy all or part of the requirement. In the following, some of the technologies under study have been presented that aim at a massive use of renewable sources, but that are today not very practicable due to the not insignificant plant complexity in relation to the modest producibility in terms of desalinated water produced.

In the second part, the SDGC system was introduced. Initially the physical structure of the plant was recalled along with the principle underlying its operation; later, the first model of calculation of the system was introduced, one of the main subjects of this document. The analysis model made it possible to relate the geometrical and thermophysical parameters to the operating conditions of the plant, allowing a simple and easy-to-use formulation to be obtained for calculating the producibility of the plant.

Based on the calculation model, it was possible to make a preliminary sizing of the most important parts, assessing any critical operating conditions and preparing the most suitable systems to counteract them. During this development phase, particular attention was paid to the standardization of the system, choosing to assemble elements commonly available in the commercial sector of the industrial sector, paying more attention to the functionality and effectiveness of the element and leaving the system optimization for future development in relation to the choice of using products and materials made to measure for a specific function. The result has led to the determination of a standard module, characterized by a good level of producibility in terms of condensed water, which could be appropriately replicated to obtain the level of productivity sought by a possible customer.

Following the sizing, an effort was made to estimate the potential costs related to the construction and operation of the plant, producing a first comparison with conventional technologies, being aware that in this first phase of development the results could be only guidance. What was achieved, however, was encouraging:

- The cost of planting was far higher than traditional plants of the same size fed through conventional sources. This is due to the non-optimization of the system according to the modularity of the SDGC system, as explained in the previous paragraph. With continued development, it is expected that this cost may fall significantly until it reaches levels comparable with conventional technologies. Furthermore, the possibility of a configuration change, aimed at obtaining a higher level of productivity than the standard model, is a precondition for achieving the desired productivity level by installing a smaller number of SDGC modules.

- Operating costs were relatively low, due to the simplicity of the plant. By purchasing electricity at an industrial price, the annual cost was relatively low. Some of the operating costs were reserved for scheduled maintenance, which consists of a total cleaning of the tanks and the removal of any salt deposits and the management of the system. For the small size of the plants, it was considered appropriate to consider the stipulation of contracts for external management, instead of hiring personnel to supervise the plant, while the increase in size was made possible by the possibility of hiring a supervisor. All this made it possible to obtain much lower operating costs compared to traditional systems of the same size, and this led to a significantly lower production cost.

6.1 System innovation

The SDGC system was found to be a potential alternative to traditional plants, as shown in section 5.5. The main innovative aspect of the system consists in reproducing, in a restricted environment, the water cycle that commonly occurs in nature. In fact, through the solar thermal energy, part of the water present in the seas and oceans evaporates according to the relationship presented in paragraph 2.2, returning towards the atmosphere. Thanks to the convective motions, the mass of water in the aeriform state is pushed up to an environment in which it condenses, thanks to the low pressures and temperatures, precipitating successively to the ground. The SDGC system exploits and accelerates this process: solar energy is used to heat the heat-carrying fluid which, by means of a heat exchanger, heats the surface of the mass of water present in the tank, making it evaporate in a closed environment in vacuum and with artificially accelerated moist air. All this allows a faster process and the

almost total recovery of latent heat thanks to the presence of the thermal tunnel. In Table 23 there was already a first positive comparison between the unit module and the orders of magnitude of the current technology park. In this section, we want to show the comparison between the system sized in the case study in paragraph 5.5 and some plants, operational and experimental, set up for the exclusive operation of solar energy, of which there is an overview in paragraphs 2.3 and 2.4, with the aim of highlighting the additional innovative and technological features of the SDGC system. Table 31 shows the declared data of the plants under examination, obtained from analysis of the scientific literature.

Technology - Installation	Size	Investment	O & M	Water cost	Energy req
	m^3/d	€	€/year	€/m^3	kWh/m^3
Solar - HDH*	0.022	1400.00	270.00	0.04–0.089	nd**
Solar - HDH*	0.02	10,775.00	1200.00	156.00	nd**
Solar - HDH*	0.5	11,440.00	80.00	4.15	nd**
ST - MED - Abu Dhabi	120	2,037,783.00	nd**	6.58	50.91
[8]ST - MED - Almeria	73	nd**	nd**	nd**	3.3 – 5
[8]PV - RO - Lampedusa	120	nd**	nd**	6.5	5.5 - 6
[8]PV - RO - BW - Ceara	8	11,300.00	654.00	10.32	4.7
[8]PV - RO-Pozo Izquierdo	3.2	nd**	nd**	9	5.5
SDGC - Case Study	**150**	**1,087,160.24**	**45,702.31**	**0.90**	**1.82**

*prototype; **undeclared

Table 31. Technical-economic data of installed systems

From this comparison, it can be deduced that the SDGC system, with a production level comparable to MED and RO plants powered by solar energy, investment costs, presents significantly lower production costs and specific consumption.

This is due to the simplicity of construction that characterizes the SDGC system; exploiting standard commonly used products reduces the costs associated with the development of new elements, which would certainly lead to an increase in the total investment cost. The modular nature of the system also allows the system to be rescaled according to the production size without completely redesigning the system, thus guaranteeing a reduced design cost.

The operation of the system allows the recovery and continuous reuse of the latent heat, making the SDGC a practically self-supplying system, since the thermal energy supplied during the start-up phase is continuously reused thanks to the presence of the thermal tunnel, unless lost through the envelope, which is reintegrated through solar collectors. This element represents the heart of the whole system and at the same time its most delicate part. In fact, it plays a dual role of equal importance: acting as a condensation and condensate collection surface and at the same time recovering the latent heat to reuse it within the system itself, allowing it to self-feed. This second function is implemented by realizing a communication path, using the procedure described in the previous sections, between the condensation zone and the exchange zone at the bottom of the tank, passing through the portion of water heated to the free surface. This solution, which in the first analysis seems simple, actually represents a great innovation, since it allows the complete recovery of the latent heat to feed the main process and not, as often happens in traditional systems, for secondary pre-heating functions. This allows a drastic reduction of the energy to be supplied to the system and, consequently, the related costs.

Thanks to these technological solutions, a specific consumption of energy is obtained that is much lower than that of the plants shown in Table 31 and allows a much lower production cost compared to alternative plants. This makes the SDGC system competitive, even with a higher investment cost, because, as shown in Table 30, it allows a return of the investment cost in a sufficiently short time, relative to the average life of this type of plant.

6.2 Future developments

The results obtained have therefore found in the SDGC system a possible alternative to the desalination methods present on the market today, setting the starting point that will allow planning of the future development of the system, as summarized below:
• Optimization of the analysis model: the model presented in the previous pages represents the very first reliable method to describe the functioning and allow a first sizing. Precisely because of its newness, it is

subject to analysis and changes that will increase the accuracy and the precision, in the direction of its final validation.

- Technical-economic optimization of the construction elements: as explained in the previous pages, for the first sizing only the effectiveness and standardization of the inserted elements was taken into consideration. Future development will necessarily have to focus on optimizing all the elements, so as to significantly reduce the cost of installation.
- Design of the plant auxiliaries: it will be necessary to provide a detailed sizing of the auxiliaries, mentioned in the project concept in paragraph 4.2.9 and of which an estimate has been made in the economic analysis in section 5. To these is added the final choice of the type of system for moving the air, described in paragraph 4.1.5, and for putting the system under vacuum.
- Complete sizing of the plant: the sizing carried out in the previous pages did not consider elements that could be complementary to the operation, such as salt-water pre-treatment systems and fresh water after-treatment systems. These sectors must necessarily be sized according to a more detailed and reliable technical and economic analysis.

The problem of the scarcity of fresh water is incredibly pressing and constantly increasing due to population growth and consumption. Investing in the development of sustainable systems for sea water desalination remains one of the key points on which it is worthwhile to concentrate our efforts to solve this problem.

References

Ayoub, G.M., & Malaeb, L. (2014) Economic feasibility of a solar still desalination system with enhanced productivity, *Desalination*, Vol. 335, No. 1, pp.27-32.

Bacha, B.H. (2013) Dynamic modeling and experimental validation of a water desalination prototype by solar energy using humidification-dehumidification process, *Desalination*, Vol. 332, pp.182-208.

Battisti, R. (2013) *Impianti solari termici per reti di teleriscaldamento*, Dario Flaccovio, Palermo.

Calza, F. (2010) *Manuale degli impianti termici e idrici*, Tecniche Nuove, Milano.

Cervinia, V.M., Masaki, O., Tetsuji, O., Satoshi, N., & Wataru, N. (2016) Effect of biofilm on inorganic suspended solids accumulation on reverse osmosis membranes, *Japan Society On Water Environment*, Vol. 14, No. 5, pp.308-318.

Chang, Z., Zheng, H., Yang, Y., Su, Y., & Duan, Z. (2014) Experimental investigation of a novel multi-effect solar desalination system based on humidification-dehumidification process, *Renewable Energy*, Vol. 69, pp.253-259.

Cipollina, A., Micale, G., Rizzuti, L (Eds.) (2009) *Seawater Desalination: Conventional and renewable energy processes*, Springer, New York.

de la Cruz, L., Cynthia, L. (2015) *Studio di fattibilità di un impianto di dissalazione ad osmosi inversa con l'utilizzo di energia solare fotovoltaica*, Politecnico di Milano, Milano.

Ducci, C. (2012) *Studio e dimensionamento di un sistema per la dissalazione e la generazione di energia con accumulo in aree rurali isolate*, Padova Digital University Archive, Padova.

El-Agouz, S.A., Abd El-Aziz, G.B., & Awad, A.M. (2014) Solar desalination system using spray evaporation, *Energy*, Vol. 76, pp.276-283.

Farina, A., Santi, A., & Lavacchielli, G. (2014) *Termofluidodinamica applicata*, Università degli studi di Parma, Parma.

Fratelli Mariani S.p.A. *Lamiera stirata in stock*, Catalogo tecnico.

Gazebo S.p.A. (2013) *Progettazione e costruzione impianti di trattamento acque reflue*, Catalogo tecnico prodotti.

Hamed, M., Kabel, A., Omara, Z., & Sharshir, S. (2014) Mathematical and experimental investigation of a solar humidification-dehumidification desalination unit, *Desalination*, Vol. 358, pp.9-17.

Kabeel, A.E., & El-Said, E.M. (2013) Applicability of flashing desalination technique for small scale needs using a novel integrated system coupled with nanofluid-base solar collector, *Desalination*, Vol. 333, No. 1, pp.10-22.

Kang, H., Yang, Y., Chang, Z., Zheng, H., & Duan, Z. (2014) Performance of a two-stage multi-effect desalination system based on humidification-dehumidification process, *Desalination*, Vol. 344, pp.339-349.

Lavanga, V., & Farné, S. (2017) *Patent n. 0001427399.*

Lavanga, V., & Farné, S. (2016) *Patent n. 102015902343234.*

Lavanga, V., & Sparacino, A.C. (2013) *Patent n. 0000275666.*

Li, X., Yuan, G., Wang, Z., Li, H., & Xu, Z. (2014) Experimental study on a humidification and dehumidification desalination system of solar air heater with evacuated tubes, Desalination, Vol. 351, pp.1-8.

Magrini, A., & Magnani, L. (2009) *Fisica Tecnica: Volume 1 - Esempi di calcolo di termodinamica e trasmissione del calore*, CittàStudi Edizioni, Torino.

Manokar, A.M., Murugavel, K.K., & Esakkimuthu, G. (2014) Different parameters affecting the rate of evaporation and condensation on passive solar still - A review, *Renewable and Sustainable Energy Reviews*, Vol. 38, pp.309-322.

Massarutto, A. (2008) *L'acqua,* Il Mulino, Bologna.

Moran, M., Shapiro, H., Munson, B., & DeWitt, D. (2011) *Introduction to thermal systems engineering,* McGraw Hill, New York.

Nam, W.K., Seockheon, L., Dooil, K., Seungkwan, H., & Ji, H.K. (2011) Analyses of calcium carbonate scale deposition on four RO membranes under a seawater desalination condition, *Water Science & Technology Journal,* Vol. 64, No. 8, pp.1573-1580.

Nematollahi, F., Rahimi, A., & Gheinani, T.T. (2013) Experimental and theoretical energy and exergy analysis for a solar desalination system, *Desalination,* Vol. 317, pp.23-31.

Pantani, R. (2010) *Effetti termici nelle trasformazioni. Principi di ingegneria chimica ambientale,* Università di Salerno, Salerno.

Park, G.L., Schafer, A.I., & Richards, B.S. (2012) The effect of intermittent operation on a wind-powered membrane system for brackish water desalination, *Water Science & Technology Journal,* Vol. 65, No. 5, pp.867-874.

Ramadan, M.R., El-Sebali, A.A., Aboul-Enein, S., & Khallaf, A.M. (2004) Experimental testing of a shallow solar pond with continuous extraction, *Energy and Buildings,* Vol. 36, No. 9, pp.955-964.

Reddy, S., & Sharon, H. (2014) A review of solar energy driven desalination technologies, Elsevier, New York.

Rognoni, M. (2010) *La dissalazione dell'acqua di mare. Descrizione, analisi e valutazione delle principali tecnologie,* Dario Flaccovio, Palerno.

Salata, F., & Coppi, M. (2014) A first approach study on the desalination of sea water using heat transformer powered by solar ponds, *Applied Energy,* Vol. 136, pp.611-618.

Schafer, A.I., Remy, C., & Richards, B.S. (2004) Performance of a small solar-powered hybrid membrane system for remote communities under varying feedwater salinities, *Water Science & Technology: Water Supply,* Vol. 5, No. 5-6, pp.233-243.

Stiferite S.r.l. (2017) *Prodotti & soluzioni per edifici efficienti,* Catalogo Tecnico.

Subramanian, S. (s.d.) *Lecture notes on the estimation of binary diffusivities,* Clarkson University, Clarkson.

Tang, M., Cox, R., & Kalberer, M. (2014) Compilation and evaluation of gas phase diffusion coefficients of reactive trace gases in the atmosphere: volume 1. Inorganic compounds, *Atmospheric Chemistry and Physics,* Vol. 14, No. 17, pp.9233-9247.

Tzen, E., Zaragoza, G., & Alarcòn Padilla, D.C. (2012) Solar Desalination, *Comprehensive Renewable Energy,* Vol. 3, pp.529-565.

UN Water (2016). *2016 UN World Water Development Report, Water and Jobs.*

World Health Organization. (2017) *Guidelines for drinking-water quality,* United Nations, Geneva.

Yildirim, C., & Solmus, I. (2014). A parametric study on a humidification-dehumidification desalination unit powered by a solar air and water heaters, *Energy Conversion and Management,* Vol. 86, pp.568-575.